Geologica Acta, Vol.8, Nº 2, June 2010, 111-130
DOI: 10.1344/105.000001526
Available online at www.geologica-acta.com

geologica acta

First evidence of lamprophyric magmatism within the Subbetic Zone (Southern Spain)

E. PUGA [1] [*] **L. BECCALUVA** [2] **G. BIANCHINI** [3] **A. DÍAZ DE FEDERICO** [1] **M. A. DÍAZ PUGA** [4] **A.M. ALVAREZ-VALERO** [1] **J. GALINDO-ZALDÍVAR** [5] **J.R. WIJBRANS** [6]

[1] **Instituto Andaluz de Ciencias de la Tierra (CSIC-UGR)**
Facultad de Ciencias, Avda. Fuentenueva s/n, 18002 Granada, Spain. Puga E-mail: epuga@ugr.es Díaz de Federico Email: adiazdef@telefonica.net Alvarez-Valero Email: antonioa@ugr.es

[2] **Dipartimento di Scienze della Terra, Università di Ferrara**
Polo Scientifico-Tecnologico - Blocco B, Via Saragat 1, 44100 Ferrara, Italy. Beccaluva E-mail: bcc@unife.it

[3] **CNR - Instituto di Geoscienze e Georisorse (IGG)**
Via G. Moruzzi 1, 56124 Pisa, Italy. E-mail: g.bianchini@igg.cnr.it

[4] **Departamento de Hidrogeología, Universidad de Almería**
Cta. Sacramento s/n, La Cañada de San Urbano, E-04120 Almería, Spain. E-mail: mdpuga@ual.es

[5] [1] **Departamento de Geodinámica, Universidad de Granada & Instituto Andaluz de Ciencias de la Tierra (CSIC-UGR)**
Avda. Fuentenueva s/n, 18071 Granada, Spain. E-mail: jgalindo@ugr.es

[6] **Department of Isotope Geochemistry, Faculty of Earth and Life Sciences**
Vrije Universiteit Amsterdam, The Netherlands. E-mail: jan.wijbrans@falw.vu.nl

* Corresponding author

ABSTRACT

Two drillings carried out at Cerro Prieto (Province of Málaga), together with additional geophysical data, revealed the existence of an igneous body formed of rock-types previously unknown in the Subbetic zone. The recovered rocks, emplaced under hypoabyssal conditions, are predominantly porphyric, containing olivine, diopside and TiO_2-rich phlogopite phenocrysts (up to 1-2 mm in size) within a micro-to-hypocrystalline groundmass composed of alkali-feldspar, diopside, phlogopite and abundant magnetite, and could be classified as "alkali minettes" lamprophyres. They contain numerous xenocrysts corroded by the magma and centimetric ultrafemic xenoliths deriving from the mantle.

Clinopyroxenes yield crystallisation temperatures from about 1150 to 1320º C and pressures ranging from about 4 to 17 kbar, suggesting 50 km as the minimum depth of the magma sources. The chemical compositions of these lamprophyres are similar to intra-plate alkali-basalts, derived from oceanic-island-basaltic-type highly metasomatized mantle sources. $^{40}Ar/^{39}Ar$ dating of a phlogopite mineral separate gave an age of 217±2.5 Ma. However, these

rocks are more similar to the Permian alkaline lamprophyres in the Spanish Central System than to the Mesozoic dolerites and basalts widespread throughout the Subbetic Zone. We propose that the Cerro Prieto subvolcanic event represents the onset of a widespread magmatic phase induced by the post-Hercynian extensional tectonic activity that also affected the whole South-Iberian Paleomargin, within a geodynamic context that ultimately led to the opening of the Atlantic and the Neotethys oceans, accompanied by intrusion of basic magmas along their continental margins.

KEYWORDS | **Lamprophyric magmatism. Metasomatized mantle. Subbetic Zone. Betic Cordilleras. Southern Spain.**

INTRODUCTION

The studied lamprophyric magmatism is present in the Subbetic Zone of the Betic Cordilleras (Fig. 1). This zone is characterized by different tectonic units mainly made up of sedimentary series (Triassic to Quaternary), which overlie the basement of the Spanish Central System. The Mesozoic Subbetic series is mainly comprised of sedimentary rocks and numerous submarine basaltic flows plus small subvolcanic dolerite bodies (Fig. 1). This magmatism changed from tholeiitic at the beginning of the Upper Triassic to transitional and alkaline sodic throughout the Jurassic, continuing intermittently until the Upper Cretaceous (Puga et al., 1988, 1989; Portugal Ferreira et al., 1995; Morata et al., 1997; Molina et al. 1998). Within this context, a small subvolcanic body of lamprohyric rocks (star in Fig. 1) was found within the Antequera Trias unit. As far as we know, this is the only example of this rock type in the whole Subbetic Zone and throughout the entire Betic Cordillera.

The aims of this study are: 1) to characterize the lamprophyres from a petrological ang geochemical point

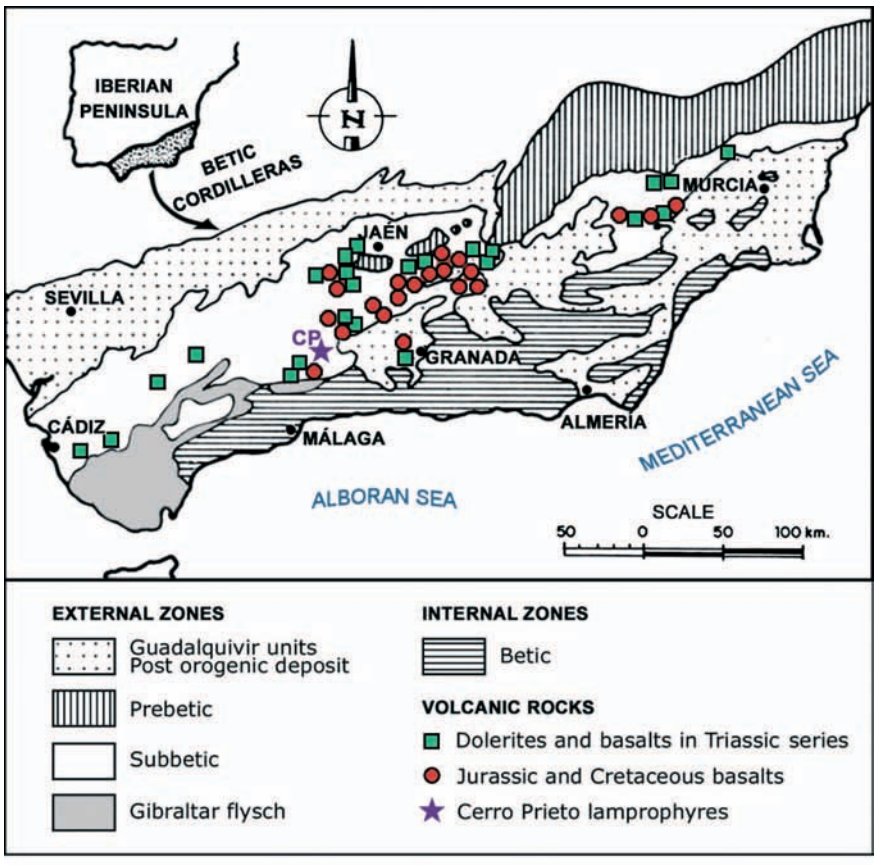

FIGURE 1 | **Location of Cerro Prieto lamprophyric outcrop within the Betic Cordilleras. The subdivision in major geotectonic zones of these cordilleras and the relative emplacement of the Mesozoic basic rocks into the Subbetic Zone are also shown, modified from Puga et al. (1989). The squares represent dolerite and minor basaltic outcrops dispersed into Triassic series and, present all along the Subbetic Zone. The circles correspond to the Jurassic-Cretaceous basaltic outcrops, which are mainly restricted to the central part of the Subbetic Zone.**

of view, 2) to determine the absolute age of this magmatic event, 3) to identify the nature of the related mantle sources and, 4) to recognise the tectonic setting that triggered the genesis of these magmas. We also try to establish the possible genetic and/or temporal relationships between this rare rock type and other magmatic occurrences of the Iberian Peninsula.

GEOLOGICAL SETTING AND CHARACTERISTICS OF THE CERRO PRIETO LAMPROPHYRES

Clues to the existence of the Cerro Prieto magmatic body could only be observed to the north of the Cerro Prieto hill (Fig. 2) where a little pile of previously excavated blocks of lamprophyres was preserved. These blocks were extracted, twenty years ago, during the perforation of a water well in the proximity of the Vivarena farmhouse, at several metres depth below surface. After a geophysical investigation a new drill (ten centimetres in diameter, fifteen metres depth) was carried out, near the water well (Fig. 2), providing direct "in situ" sampling of the lamprophyric rocks.

The Cerro Prieto lamprophyres are geologically located in the Antequera Trias unit of the Subbetic Zone (Figs. 1 and 2). This domain forms part of the external zones of the Betic Cordillera, which in turn represents the westernmost part of the Mediterranean Alpine Belt. The Antequera Trias unit is composed of a tectonic "mélange" with extremely tectonized, hectometric blocks of Triassic to Tertiary age that have been affected by notable diapiric processes and are covered by an olistostromic formation (Sanz de Galdeano et al., 2009). Some of these blocks have been affected by a few pervasive low grade metamorphism in prehnite-pumpellyite to actinolite-pumpellyite facies during the Alpine orogeny (Puga et al, 1983, 1988, 1989, 2004; Aguirre et al., 1995), which also affected the Cerro Prieto magmatic body.

The lamprophyric rocks forming the Cerro Prieto magmatic body seem to have been inserted into clayey sediments, which form, together with limestone and gypsum, part of the extremely tectonised Upper Triassic series of the Antequera Trias (Fig. 2). These intrusive rocks do not, however, show clear direct contact with the host series because they are mainly covered by Holocene deposits.

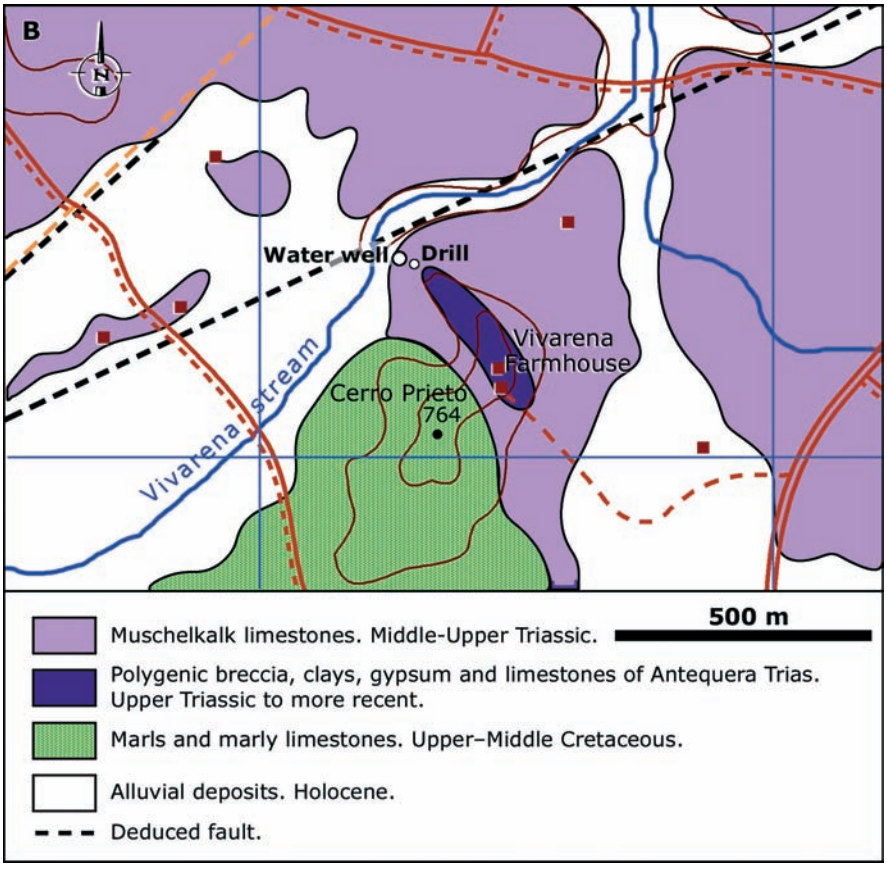

FIGURE 2 | **Geological schematic map of the Cerro Prieto area, located at about 5 km to the SE of Archidona village (Málaga province), showing the emplacement of the water well and the drill from which the studied samples were extracted. Figure following the geological map 1:50.000 of the MAGNA series corresponding to Archidona (nº 1024) (Pineda Velasco, 1990).**

ANALYTICAL METHODS

Magnetic measurements were made with a GSM-8 precession magnetometer to an accuracy of 1 nT. The positions of the measurement stations were determined by GPS and their height by a barometric altimeter with a precision of 0.5 m. The magnetic anomaly obtained, after diurnal and IGRF corrections, is shown in the map in Fig. 3A. The samples of basic rocks were analyzed with an Exploranium KT-5 susceptibility meter. To establish the geometry of the body in greater detail a N-S model orthogonal to the main dipole (Fig. 3B) was calculated with Gravamag 1.7 software (Pedley et al., 1993).

Mineral compositions were obtained with a CAMECA SX50 electron microprobe (University of Granada) operating at 20 kV and 20 nA; synthetic SiO_2, Al_2O_3, $MnTiO_3$, Fe_2O_3, MgO and natural diopside, albite and sanidine were used as standards. Fe^{3+} in clinopyroxene was calculated after normalization to 4 cations and 6 oxygens (Droop, 1987) per formula unit (pfu).

Major-element and Zr concentration were determined on glass beads made of 0.6g of powdered sample diluted in 6g of $Li_2B_4O_7$ using a PHILIPS Magix Pro (PW-2440) X-ray fluorescence (XRF) spectrometer at the "Centro de Instrumentación Científica" (CIC) of Granada University. Precision was better than ± 1.5% for an analyte concentration of 10 wt%. Precision for Zr was better than ± 4% at a concentration of 100 ppm. Trace elements other than Zr were determined at the University of Granada (CIC) by ICP-mass spectrometry (ICP-MS) using a PERKIN ELMER Sciex-Elan 5000 spectrometer; sample solutions were prepared digesting 0.1 g of sample powder with HNO_3 + HF in a Teflon-lined vessel at ~180ºC and ~200 p.s.i. for 30 min, subsequently evaporating to dryness and dissolving in 100 ml of 4 vol% HNO_3. The concentrations of the international standards PM-S and WS-E run were not significantly different from the recommended values (Govindaraju, 1994). Precision was better than ± 5% and ± 2% for concentrations of 5 and 50 ppm.

Sr-Nd isotope analyses were carried out at the University of Granada (CIC), where whole-rock samples were digested as described for the ICP-MS analysis, using ultra-clean reagents, and analysed by thermal ionization mass spectrometry (TIMS) using a Finnigan Mat 262 spectrometer after chromatographic separation with ion exchange resins. Normalization values were $^{86}Sr/^{88}Sr = 0.1194$ and $^{146}Nd/^{144}Nd = 0.7219$. Blanks were 0.6 and 0.09 nanograms for Sr and Nd respectively. External precision (2σ), estimated by analysing 10 replicates of the standard WS-E (Govindaraju, 1994), was better than 0.003% for $^{87}Sr/^{86}Sr$ and 0.0015% for $^{143}Nd/^{144}Nd$. The measured $^{87}Sr/^{86}Sr$ of the NBS 987 international standard was 0.710250 ±

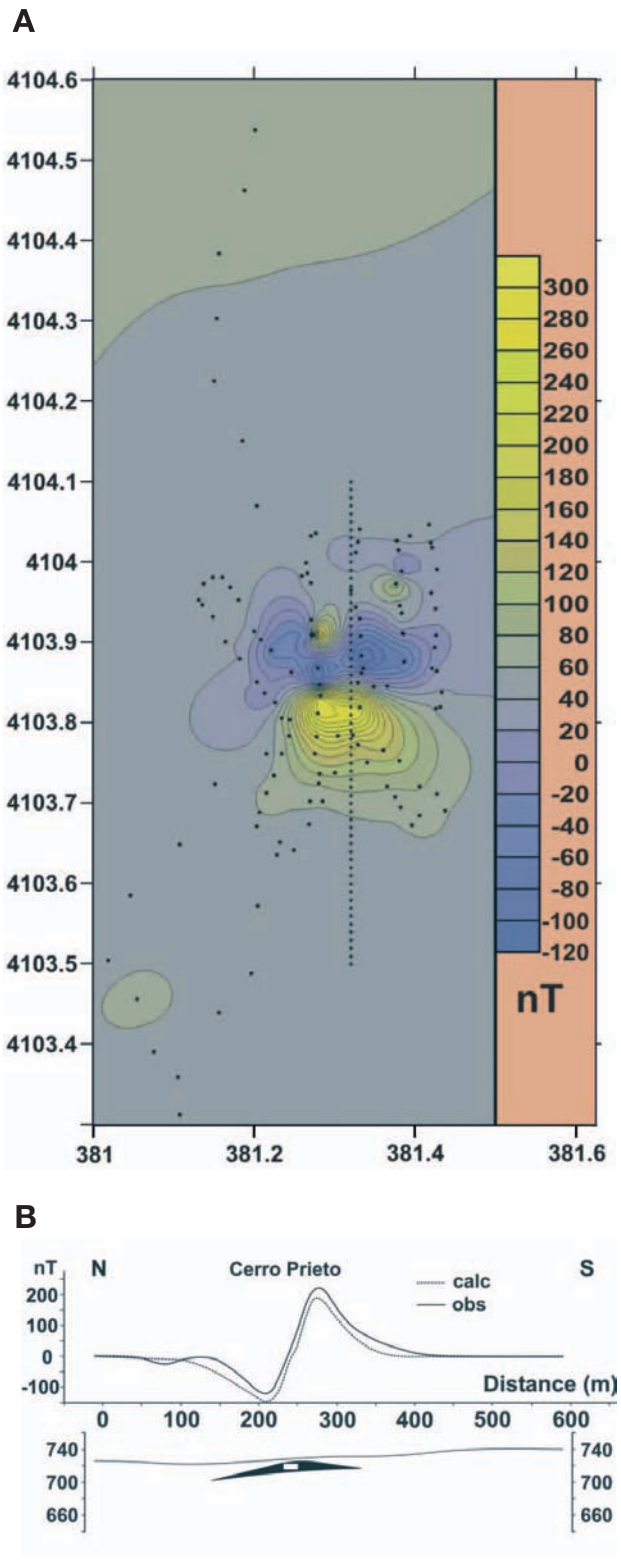

FIGURE 3 | **A) Map of total field magnetic anomaly (nT) in Cerro Prieto area with coordinates in UTM. Dots correspond to position of measurement stations. Dotted line indicates the position of the magnetic model represented in part B of the Figure; B) Model of total field magnetic anomaly following the dotted line on the previous Figure. In black is schematically shown the lenticular magmatic body located very near of the surface. Susceptibility of anomalous body attributed to basic igneous rocks is 0.045 SI.**

0.0000044, whereas measurements of the La Jolla Nd international standard yield a $^{143}Nd/^{144}Nd$ ratio of 0.511844 ± 0.0000065.

$^{40}Ar/^{39}Ar$ incremental heating experiments were carried out in the geochronology laboratory at the Vrije Universiteit, Amsterdam. The groundmass samples were crushed and sieved and the sieved fractions were washed and ultrasonically cleaned to remove surface intergrowths. The 250 - 500 μm fraction was used for dating. The phlogopite sample was separated at the University of Granada. The phlogopite concentrates were prepared by crushing, sieving, flotation and handpicking of grains with sizes of 100 - 250 μm, which were used for dating. About 40 mg of each sample was packed in 9-mm-diameter aluminium-foil packages and stacked with packages containing a mineral standard in a 10 mm OD quartz tube. The mineral standard was DRA-1 sanidine with a K/Ar age of 25.26 Ma. The quartz vial was packaged in a standard aluminium irradiation capsule and irradiated for 12 hrs (groundmass - VU54) and 18 hrs (phlogopite - VU62) in a cadmuim-lined rotating facility (RODEO) at the NRG-Petten HFR facility in The Netherlands. Once returned to the Amsterdam laboratory, samples were analyzed following the procedure outlined in Wijbrans et al. (2007). During the course of the project the argon ion laser was decommissioned and replaced by a CO_2 laser. For the second experiment the sample house was fitted with a 49 mm diameter ZnS dual vacuum UHV window. Positioning of the laser beam was achieved using an analogue Raylease scanhead fitted with a dual mirror system for X-Y adjustment and a ZnS 300 mm focussing lens. The beam delivery system achieved a ca. 300 micrometer at the focal point. For the phlogopite approximately 5 mg of sample was used for the experiment, whereas for the groundmass approximately 20 mg. System blanks were found to be stable and predictable during the runs. Sample to blank ratios for the ^{40}Ar ion-beam were systematically well in excess of 100 for the larger and older age steps.

GEOPHYSICAL CONSTRAINTS

Geophysical techniques were used to determine the extension and geometry of the Cerro Prieto igneous intrusion. The studied area (near the water well in Fig. 2), shows an overprinting of high-density basic rocks and limestones, and low-density gypsum and clays, which prevent the use of gravity techniques. Nevertheless, a magnetic survey revealed a high contrast between the magnetic properties of the igneous rocks and those of the host rocks, thus allowing us to establish the main features of its structure.

A main magnetic dipole about 300 m long is associated with the igneous body, with maximum and minimum values of 300 nT and -120nT (Fig. 3A). Small irregularities should appear at its northern and north-eastern edges, as revealed by the presence of local dipoles. The high variability and intensity of the magnetic anomalies support the idea that this is a shallow "anomalous" body. The maximum is located to the south and the minimum to the north, indicating that this anomaly may be modeled as contrast in magnetic susceptibility. Any remnant magnetism should run subparallel to the magnetic induction. Taking into account the mean susceptibility value, determined as 0.045 SI for the basic igneous rocks, and the position of the top of the body in the drilling and the water well, the theoretical and measured magnetic anomalies suggest the presence of a lenticular body characterized by a maximum thickness of 10 - 15 m and an approximate length of 200 m (Fig. 3B).

Magnetic surveys of the surrounding area (Fig. 3A) found no evidence of any other nearby magnetic anomalies, suggesting that this magmatic body is isolated. Nevertheless, a previous geophysical study carried out in the locality of Archidona, near Cerro Prieto, revealed the existence of a kilometric body of basic rocks at a depth of ca. 5 to 18 km (Bohoyo et al., 2000) that might be genetically related to the small, shallow manifestation of the Cerro Prieto magmatism.

PETROGRAPHY

Subvolcanic rocks

A petrographical study of the magmatic rocks drilled at Cerro Prieto indicated that they were emplaced very close to the surface. This is suggested by: a) the rock textures, which are mainly porphyritic with abundant golden-brown millimetric phenocrysts of phlogopite in a black aphanitic groundmass, and b) the subordinate presence of pyroclastic material in the upper part of the subvolcanic body. The investigated rocks are very homogeneous, containing olivine (often chloritized), diopside, and TiO_2-rich phlogopite phenocrysts up to 1-2 mm in size, within a micro-to-hypocrystalline matrix composed by alkali-feldspar, diopsidic clinopyroxene, phlogopite and abundant magnetite (Fig. 4, photo). According to their texture and modal composition, these rocks can be classified as olivine-phlogopite-sanidine-bearing lamprophyres. This lamprophyre type is difficult to classify using Le Maitre et al. (1989) and Rock et al. (1991) schemes, due to its modal similitude with a calc-alkaline minette despite its alkaline chemical character. In this light, these lamprophyres, might more properly be termed "alkali minettes", following the criterion of Wooley et al. (1996) and the IUGS recommendations.

The Cerro Prieto lamprophyres are the only known occurrence among the magmatic rocks of the Subbetic Zone (Fig. 1). The most notable mineralogical peculiarities that distinguish these lamprophyres from other types of igneous rocks present in the Subbetic Zone are: a) the absence of calcic plagioclase and the presence of alkaline feldspar (Fig. 5), and b) the abundant igneous TiO_2-rich phlogopite, which is not present in the Mesozoic dolerites and basalts. Other minerals such as olivine and clinopyroxene are common in all these types of rocks, although presenting some textural and minor chemical differences (Fig. 6).

Xenocrysts and xenoliths

The Cerro Prieto lamprophyres also contain numerous millimetric to centimetric xenocrysts and xenoliths both of mantle and crustal origin. These fragments of foreign minerals and rocks were entrained by the lamprophyric magma and are generally surrounded by millimetric reaction coronas of different compositions. The more common xenocrysts are megacrysts of partly sericitized plagioclase, apatite, clinopyroxene, ferrian spinel and, to a lesser extent, tectonised quartz. The xenoliths consist of carbonate rocks, dolerites (sometimes containing phlogopite) and different types of ultramafic rock. Hand-specimen and optical microscope observations reveal that the different xenocryst and xenolithic types may be present in a single lamprophyre sample.

Millimetric inclusions of polycrystalline calcite surrounded by big crystals of Ti-rich phlogopite are common in the Cerro Prieto lamprophyres. They could

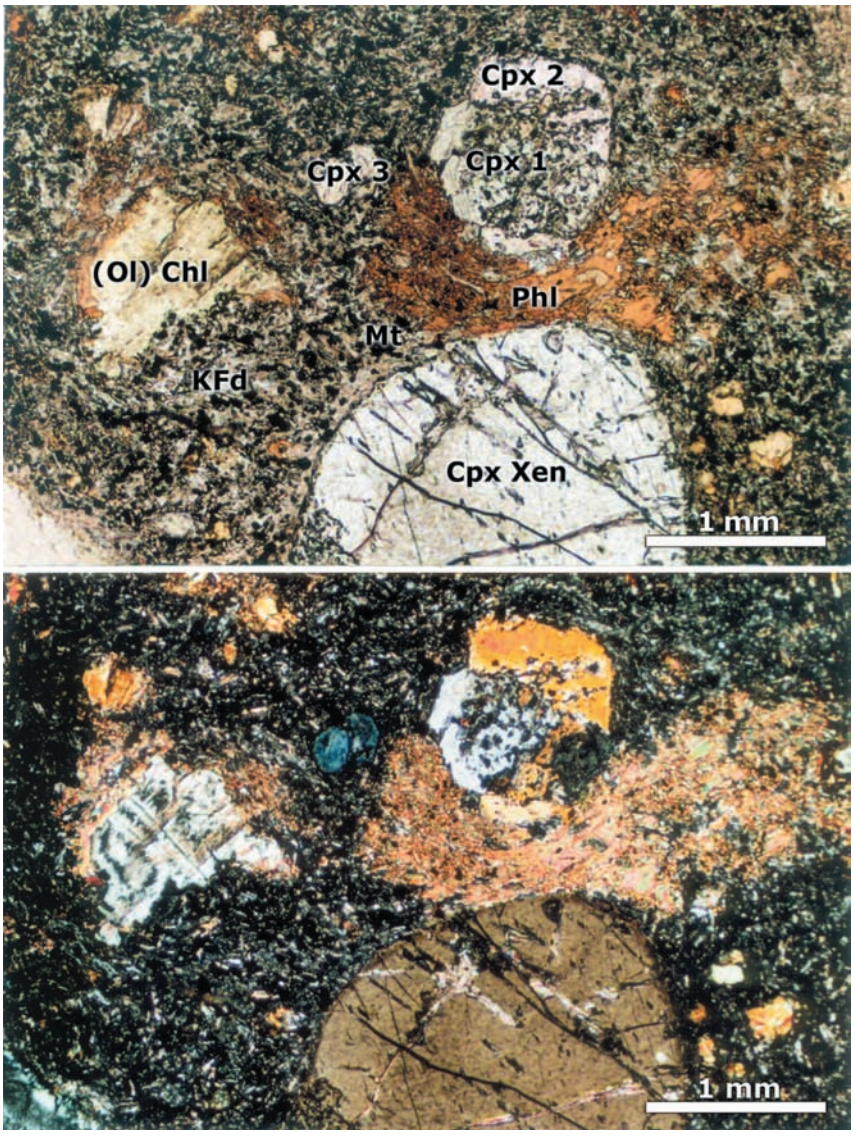

FIGURE 4 | **Optical microscopic photographs (plane-polarized at the top and crossed-nichols at the bottom) of a representative thin section of the Cerro Prieto lamprophyres. The photos show: Diopsidic clinopyroxene phenocrysts (Cpx 1 and 2) and microphenocrysts (Cpx 3), and olivine phenocrysts pseudomorphized by chlorite (Chl) and surrounded by phlogopite crystals (Phl), in a matrix formed by black magnetite, interlocked with alkali-feldspars, diopside and phlogopite. A small part of a centimetric Al-rich diopside xenocryst (Cpx Xen) is also shown in the lower part of the microphotographs. Mineral abbreviations following Kretz (1983).**

represent segregation ocelli, which would suggest that the related magma was very rich in both CO_2 and H_2O. Surrounding the carbonate inclusions, reaction coronas including hydro-andradite garnet and diopside have been developed at the contact with the large phlogopite crystals and the host magma.

Centimetric ultramafic xenoliths, consisting mainly of millimetric crystals of Al-rich diopside associated with minor Fe-spinel, are very common and could represent high-pressure cumulates crystallized in deep magmatic chambers. A further type of ultramafic xenoliths (several centimetres in length) consists of mantle-derived Cr-spinel and Cr-diopside, together with pseudomorphs of orthopyroxene, garnet and olivine (replaced by phyllosilicates). These are surrounded by a calcite matrix with abundant hydro-andradite. They are also characterized by the presence of rounded aggregates, up to one centimetre in diameter, formed by symplectitic textures, consisting of an intimate association of pyroxenes and vermicular crystals of chromian spinel. Similar symplectitic intergrowths have been interpreted by different authors as the result of garnet destabilization in mantle peridotites giving way to enstatite-hosting vermicular exsolution of chromian spinel and diopside (Mercier and Nicolas, 1975; Piccardo et al., 2004).

The Cerro Prieto magmatic body has also been affected by very-low-grade Alpine metamorphism, in prehnite-pumpellyite to pumpellyite-actinolite facies, probably at the beginning of the Paleogene. This metamorphism developed a non pervasive blastesis of prehnite, pumpellyite, epidote and sericite, which overprinted the primary parageneses of the lamprophyres and their enclosed xenoliths. It is plausible that the peculiar presence of hydro-andradite garnet in some samples is related to these metamorphic reactions. The metamorphic minerals are mainly associated with calcite, which also fills some millimetric vesicles and microfissures cross-cutting both lamprophyres and xenoliths.

MINERAL CHEMISTRY

The Cerro Prieto lamprophyres are mineralogically quite homogeneous, although clinopyroxenes and alkali-feldspars show a great variety of textural relations and variable chemical compositions (Figs. 5 and 6 and Tables 1 and 2). Other primary minerals, such as phlogopite, olivine and magnetite, present no major variations in textures and composition (Table 3).

Feldspars in different textural relations range in composition from albite to orthoclase with very small quantities of anorthite (An_{2-7}) (Fig. 5). Feldspars forming the microphenocrysts and the matrix of the lamprophyres vary from potassic sanidine to albite (Table 1). The highest calcic composition is shown by relics of plagioclase xenocrysts (centimetric in size), which show an oligoclase composition (An_{20-25}) rimmed by sericitized zones. The feldspars of reaction coronas also plot along the variation range from the sodic to potassic end-members. The compositions of representative calcic plagioclases (An_{50-70}) from the Mesozoic dolerites and basalts of the Subbetic zone are also shown for comparison in Fig. 5 and Table 3.

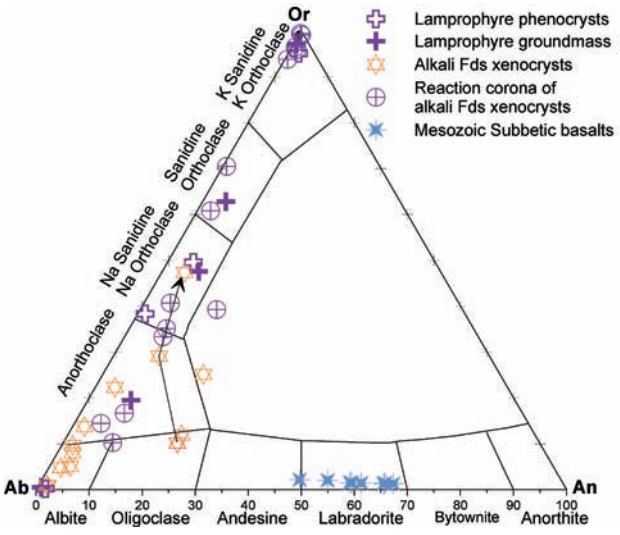

FIGURE 5 | **End-members composition of the alkali-feldspars of the Cerro Prieto lamprophyres, in various textural relations. They contrast with the labradoritic composition of the Triassic to Cretaceous basalts of the Subbetic Zone.**

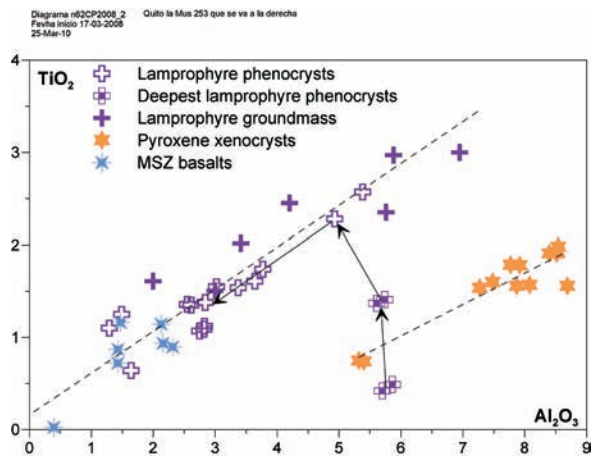

FIGURE 6 | **TiO_2 vs. Al_2O_3 variations of the different textural types of diopsides from the Cerro Prieto lamprophyres. They highlight different crystallisation conditions, compared to the more restricted compositional range shown by the augites of the Triassic to Cretaceous basalts of the Subbetic Zone. The arrows join different clinopyroxene present in the same sample.**

TABLE 1 | **Electron microprobe analyses and calculated cations of feldspars from Cerro Prieto lamprophyres (nº 1 to 7) and MSZ basalts (nº 8).**

Nº	1	2	3	4	5	6	7	8
Sample	CPr6/30	6,50/17,10	CPr3/24	CPr6/1	PR-XC-1	PR-XC-1	CPr6/4	PR-Of/23
Mineral	Na Sanidine	K Sanidine	Na Sanidine	Sanidine	Oligoclase	Na Sanidine	Anorthoclase	Labradorite
Textural relation	Phenocryst		Groundmass		Xenocryst		Reaction corona	Phenocryst
wt%								
SiO_2	64.10	61.18	64.07	63.36	62.06	54.66	65.03	52.49
TiO_2	0.16	0.12	0.31	0.19	0.05	0.09	0.02	0.08
Al_2O_3	19.31	17.67	19.69	19.13	22.93	28.20	20.10	29.36
FeO	0.31	0.30	0.27	0.47	0.17	0.45	0.05	0.63
MnO	0.02	0.00	0.01	0.02	0.00	0.00	0.00	0.01
MgO	0.00	0.00	0.01	0.01	0.00	0.12	0.00	0.11
CaO	0.97	0.09	1.31	0.69	4.25	0.08	1.35	12.43
Na_2O	5.18	0.32	5.16	3.75	7.76	4.17	6.43	4.36
K_2O	8.58	15.81	8.20	10.89	1.76	6.21	5.93	0.26
F	0.00	0.12	0.00	0.00	0.00	0.00	0.00	-
Cl	0.00	0.30	0.07	0.18	0.00	0.01	0.14	-
BaO	0.35	0.58	0.11	0.16	-	-	-	-
Total	99.01	96.51	99.20	98.84	98.98	93.99	99.05	99.73
Cations calculated on the basis of 8 oxygens								
Si	2.938	2.979	2.924	2.939	2.788	2.604	2.939	2.394
Ti	0.006	0.004	0.011	0.007	0.002	0.003	0.001	0.003
Al	1.043	1.014	1.059	1.046	1.214	1.583	1.070	1.578
Fe*	0.012	0.012	0.010	0.018	0.006	0.018	0.002	0.024
Mn	0.001	0.000	0.000	0.001	0.000	0.000	0.000	0.000
Mg	0.000	0.000	0.000	0.000	0.000	0.009	0.000	0.008
Ca	0.048	0.005	0.064	0.034	0.204	0.004	0.065	0.608
Na	0.461	0.030	0.457	0.337	0.676	0.386	0.563	0.386
K	0.502	0.982	0.477	0.645	0.101	0.378	0.342	0.015
Ba	0.006	0.011	0.002	0.003	-	-	-	-
End-members								
Or	49.31	94.66	47.48	62.70	10.20	47.35	35.13	1.46
Ab	45.26	2.91	45.44	32.79	68.27	48.36	57.87	37.95
An	4.82	2.43	6.87	4.51	21.53	4.29	7.00	60.59

Fe* = Total iron as Fe2+. End members following Deer et al. 1992

TABLE 2 | **Electron microprobe analyses and calculated cations of clinopyroxenes from Cerro Prieto lamprophyres (nº 1 to 9) and MSZ basalts (nº 10).**

Nº	1	2	3	4	5	6	7	8	9	10
Sample	1,62/29,26	1,62Nar,20	1,62Nar,21	1,62Nar,22	CPr-3,40	CPr-3/24	CPR-4/16	CPr-6,1	CPR-4,29	15,51/F8,1
Mineral	Diopside	Diopside	Diopside	Diopside	Diopside	Diopside	Diopside	Al-rich diopside	Al-rich diopside	Augite
Textural relation	Phenocr. 1	Phenocr. 2	Phenocryst 3		Groundmass			Xenocryst		Phenocryst
wt%										
SiO_2	51.60	48.88	49.73	47.14	46.82	53.07	46.07	47.70	47.44	52.57
TiO_2	0.49	1.37	1.38	2.28	2.97	0.42	3.00	1.98	2.01	0.72
Al_2O_3	5.86	5.61	2.84	4.93	5.88	0.14	6.95	8.54	8.52	1.43
Cr_2O_3	1.01	0.71	0.16	0.07	0.07	0.00	0.51	0.00	0.01	0.26
FeO*	4.12	6.84	7.87	9.09	8.23	6.68	7.76	5.82	6.17	9.71
MnO	0.11	0.13	0.11	0.16	0.16	0.16	0.11	0.10	0.16	0.23
MgO	15.52	14.51	14.82	12.90	12.90	15.89	12.71	13.01	12.63	17.31
CaO	19.87	20.34	21.49	21.55	20.85	22.26	20.70	20.99	20.04	17.71
Na_2O	1.43	0.70	0.36	0.54	0.67	0.49	0.42	0.97	1.07	0.25
K_2O	0.01	0.03	0.03	0.03	0.04	0.01	0.01	0.00	0.01	0.02
F	0.14	0.17	0.19	0.16	0.14	0.01	0.05	0.00	0.09	0.15
Cl	0.00	0.01	0.00	0.01	0.02	0.00	0.02	0.00	0.00	0.00
Total	100.21	99.38	99.05	98.89	98.79	99.16	98.37	99.11	98.19	100.37
Cations calculated on the basis on six oxigens, with Fe^{3+} after Droop (1987) and normalizated to 4 cations										
Si	1.868	1.814	1.862	1.781	1.767	1.969	1.747	1.767	1.779	1.936
Ti	0.013	0.038	0.039	0.065	0.084	0.012	0.086	0.055	0.057	0.020
Al	0.250	0.245	0.125	0.219	0.262	0.006	0.311	0.373	0.376	0.062
Cr	0.029	0.021	0.005	0.002	0.002	0.000	0.015	0.000	0.000	0.008
Fe^{3+}	0.074	0.101	0.117	0.148	0.102	0.070	0.047	0.053	0.041	0.055
Fe^{2+}	0.051	0.111	0.129	0.139	0.157	0.138	0.199	0.127	0.152	0.244
Mn	0.003	0.004	0.003	0.005	0.005	0.005	0.004	0.003	0.005	0.007
Mg	0.838	0.803	0.827	0.726	0.726	0.879	0.719	0.718	0.706	0.950
Ca	0.771	0.809	0.862	0.872	0.843	0.885	0.841	0.833	0.805	0.699
Na	0.100	0.050	0.026	0.040	0.049	0.036	0.031	0.070	0.078	0.018
K	0.000	0.001	0.001	0.001	0.002	0.000	0.000	0.000	0.000	0.001
#mg	*0.94*	*0.88*	*0.86*	*0.84*	*0.82*	*0.86*	*0.78*	*0.85*	*0.82*	*0.80*
End-members										
Wo (Ca)	46.84	46.83	47.32	50.04	46.98	46.41	46.49	49.53	47.09	36.77
En (Mg)	50.93	46.49	45.40	41.68	36.47	46.10	39.72	42.71	41.29	50.00
Fs (Fe+Mn)	2.23	6.68	7.28	8.27	16.55	7.49	13.80	7.76	11.61	13.23

FeO*.- All iron as FeO; #mg = MgO/(MgO+FeO*) mol; end-members following Deer et al. (1992).

TABLE 3 | **Electron microprobe analyses and calculated cations of mica, olivine, and spinel and apatite from phenocrysts and xenocrysts of Cerro Prieto lamproyres.**

Nº	1	2	3		4	5	6	7	9
Sample	CPR-4,33	6,43,17	CPr6,4		CPr-3,32	CPr-3,31	CPR-4/16	CPR-4/13	PrXc-1
Mineral	Ti-Phlogopite	Ti-Phlogopite	Ti-Phlogopite		Chrysolite	Chrysolite	Aluminian Mt	Ferrian Spinel	Apatite
Textural relation			Phenocrysts					Xenocrysts	
Wt%									
SiO_2	37.26	37.54	38.65		38.43	39.24	0.47	0.06	0.42
TiO_2	8.30	8.54	7.44		0.04	0.00	3.17	0.13	0.00
Al_2O_3	13.38	12.77	13.10		0.02	0.01	1.38	60.02	0.08
Cr_2O_3	0.03	0.00	0.00		0.00	0.00	0.23	0.02	0.00
FeO	10.15	10.18	8.37		22.88	18.66	83.64	23.43	0.23
MnO	0.08	0.09	0.10		0.44	0.28	0.05	0.16	0.13
MgO	16.29	16.81	18.44		38.48	42.12	0.09	14.25	0.11
CaO	0.05	0.03	0.04		0.25	0.12	0.34	0.00	51.97
Na_2O	0.59	1.15	0.54		0.01	0.01	0.02	0.00	0.10
K_2O	9.20	8.55	9.44		0.00	0.00	0.12	0.00	0.06
F	0.73	1.36	0.67		0.00	0.11	0.23	0.04	3.62
Cl	0.18	0.11	0.09		0.01	0.01	0.00	0.01	2.37
P_2O_5	-	-	-	-	-	-	-	-	40.75
Total	96.52	97.43	97.05		100.70	100.73	89.96	98.37	100.00
Cations on basis of		*22 Oxygen*			*4 Oxygen*		*4 Oxygen*		*12.5 Oxygen*
Si	5.511	5.561	5.606		0.997	0.999	0.013	0.002	-
Ti	0.923	0.951	0.811		0.001	0.000	0.065	0.003	0.000
Al	2.332	2.229	2.239		0.001	0.000	0.045	1.850	0.008
Cr	0.004	0.000	0.000		0.000	0.000	0.005	0.000	0.000
Fe^{3+}	0.157	0.210	0.154		-	-	1.843	0.145	-
Fe^{2+}	1.099	1.051	0.860		0.496	0.397	0.996	0.440	0.018
Mn	0.010	0.011	0.012		0.010	0.006	0.001	0.003	0.010
Mg	3.592	3.712	3.988		1.488	1.598	0.004	0.555	0.015
Ca	0.008	0.005	0.006		0.007	0.003	0.010	0.000	5.216
Na	0.169	0.330	0.152		0.001	0.000	0.001	0.000	0.018
K	1.736	1.616	1.747		0.000	0.000	0.004	0.000	0.007
P	-	-	-		-	-	-	-	3.176
Siderophyllite	24.69	24.91	21.45	Fo	75.11	80.16			
Annite	11.46	10.24	8.23	Fa	24.89	19.84			
Phlogopite	63.85	64.85	70.32						

End-members following Deer et al. (1992); FeO* = All iron as Fe^{2+}.

Clinopyroxene is diopside and minor diopsidic augite (Morimoto et al., 1988), and highlights compositional differences between most of phenocrysts, groundmass microcrysts and xenocrysts (Fig. 6 and Table 2). Accordingly, in a Ti vs. Al plot clinopyroxenes show two trends, one corresponding to the phenocrysts and groundmass microcrysts and the other to the xenocrysts. Some rare phenocrysts of the lamprophyres (the "deepest lamprophyre phenocrysts" in Fig. 6) have higher Al_2O_3/TiO_2 and plot near the field of clinopyroxene xenocrysts, suggesting different crystallization conditions.

THERMOBAROMETRIC CONSTRAINTS

The temperature (T) and pressure (P) of crystallisation of the Cerro Prieto lamprophyres were investigated using the new clinopyroxene thermobarometer of Putirka (2008). The thermometer (eqn. 32d in Putirka, 2008), provides results ranging from 1157 to 1323 (±16) ºC. The barometer (eqn. 32b in Putirka, 2008), based on the Nimis (1995) model, considers the presence of H_2O in the liquid in equilibrium with the clinopyroxene, and gives results in the range of 3.6 - 16.6 (±1.4) kbar.

The clinopyroxene phenocrysts identified in Fig. 6 as "deepest phenocrysts" may be subdivided into two groups according to their crystallisation pressure, and are referred to as "lamprophyre phenocrysts 1 and 2" in Table 4. The P average values corresponding to group 1 are about 16 kbar (ca. 50 km depth), while those corresponding to group 2 are about 10 kbar (ca. 30 km depth). Moreover, the most common lamprophyre phenocrysts, forming the group "lamprophyre phenocrysts 3" in Table 4, show P crystallisation conditions ranging from 3.6 to 8.2 kbar (11 to 25 km depth). Finally, P values calculated for the clinopyroxene xenocrysts vary from c. 13 to 16 kbar (about 38 to 48 km of depth). All these types of clinopyroxene and their textural relationships are shown in the microphotography of Fig. 4.

The previously exposed data show that the Cerro Prieto lamprophyres include clinopyroxenes formed at various depths, reflecting a multi-stage (polybaric) crystallisation process, from mantle depths toward a shallow level emplacement at crustal conditions. The maximum P values calculated for the lamprophyre phenocrysts 1, corresponding to 16.6 kbar, also constrain the minimum depth of magma genesis to ca 50 km.

TABLE 4 | **Results of thermobarometry for Cerro Prieto clinopyroxene in different textural relations using the calibration of Putirka, 2008.**

Sample	Cpx	Rock type	T (ºC)	P (kbar)	* Depth (km)
Pr-SK-2a,49	augite	lamproph. phenoc. 3	1172	3.6	11
CPR-4/16,34	diopside	lamproph. phenoc. 3	1157	6.3	19
CPR-4/16,28	augite	lamproph. phenoc. 3	1198	7.6	23
CPR-4/16,27	diopside	lamproph. phenoc. 3	1175	8.2	25
			avg. 1176±17	avg. 6±1.9	avg. 19±6
1,62Nar,19	diopside	lamproph. phenoc. 2	1234	9.7	29
1,62Nar,20	diopside	lamproph. phenoc. 2	1236	9.9	30
			avg. 1235±1	avg. 10±0.1	avg. 29
1,62/29,25	diopside	lamproph. phenoc. 1	1323	16.2	49
1,62/29,26	diopside	lamproph. phenoc. 1	1323	16.6	50
			avg. 1323	avg. 16±0.3	avg. 49±1
PrXc2/18,21	diopside	clinopyroxene xenocryst	1221	12.8	38
CPr6/12,1	diopside	clinopyroxene xenocryst	1234	13.4	40
CPR-4/13,31	diopside	clinopyroxene xenocryst	1251	14.6	44
PrPz/16,34	diopside	clinopyroxene xenocryst	1253	15.0	45
PirPr1/11,1	diopside	clinopyroxene xenocryst	1272	15.9	48
			avg. 1246±20	avg. 14±1.2	avg. 43±3

* Depth estimates considering an average *lower crust-upper mantle* pressure gradient = 3 km/kbar

BULK-ROCK GEOCHEMISTRY

The Cerro Prieto lamprophyres are characterized by the ubiquitous presence of abundant xenocrysts and xenoliths, which have been carefully eliminated by hand-picking under the binocular microscope to obtain a reliable and representative composition of the host lamprophyric rocks that is reported in Tables 5A and 6.

The *mg* number (MgO/(MgO+FeO*) of these rocks varies from 0.50 to 0.60. Their TiO_2 and P_2O_5 contents are high, ranging from 1.8 to 2.2 and 0.4 to 0.6 respectively, and their K_2O/Na_2O ratios range from 0.5 to 5.1 with an average value of 1.45 (Table 5A). These chemical characteristics correspond to lamprophyric rocks derived from basaltic to trachybasaltic magmas with alkaline character. The L.O.I. for these rocks, ranging from about 2 to 4 (Table 5A), is mainly due to the presence of igneous phlogopite, together with minor secondary hydrous phases, such as chlorite that pseudomorphize olivine.

In order to recognise possible genetic relationships between the rare Cerro Prieto lamprophyres and other magmatic occurrences of the Iberian Peninsula, spatial or mineralogically related, we compared (Table 5B and Figs. 7 to 11) their chemical compositions with those of the Mesozoic magmatism of the Subbetic Zone (MSZ), the post-Hercynian lamprophyres of the Spanish Central System (SCS), and the lamproites and alkali basalts of the Neogene magmatic province of south-east Iberian Peninsula (SEIP).

The Cerro Prieto lamprophyres plot in the alkaline field of the total alkali-silica diagram (Le Bas et al., 1986), with compositions mainly ranging from trachybasalt (TB) to basaltic trachyandesite (BTA) (Table 5A). Coherently, they plot also within the alkali-basaltic magma field on the Zr/TiO_2 *vs*. Nb/Y diagram (Fig. 7), and show higher similarity with the SCS lamprophyres and the SEIP alkali basalts than to the SEIP lamproites or the MSZ basalts and dolerites. In the Th/Yb *vs*. Nb/Yb diagram (Fig. 8), the Cerro Prieto lamprophyres plot in the upper part of the MORB-OIB array field, also showing analogies with the SCS lamprophyres. The high Th/Yb of the Cerro Prieto lamprophyres (close to the upper limit of the mantle array field) is mainly due to a remarkable Yb depletion with respect to the other rock types (Tables 5A and B). The MSZ basalts and dolerites show lower Th/Yb mainly due to their higher Yb content, and the SEIP lamproitic magmas plot farther away from the mantle array field due to much higher Th content (Table 5B). Therefore, these diagrams indicate that compositions of the Cerro Prieto lamprophyres closely match those typical of anorogenic mantle derived melts unaffected by crustal contamination processes (Pearce, 1982).

The Chondrite-normalized rare-earth-element (REE) patterns of Cerro Prieto lamprophyres are very steep (Fig. 9), with $(La/Lu)_N$ varying from 15 to 30, i.e. higher than in the other considered rock types, with the exception of the SEIP lamproites. These fractionated REE trends conform to the average value of OIB basalts (Sun and McDonough, 1989), and are also observed in

TABLE 5 A | **Representative major and trace element whole-rock analyses of Cerro Prieto lamprophyres.**

Nº	1	2	3	4	5	6	7
Label	3.32 CP	PIR-PR-1	PR-PX	6.43 CP m	14.21 CP	PR-PZ-6	6.5 CP
SiO_2 (wt%)	47.41	48.90	47.52	49.55	46.93	48.85	49.26
TiO_2	1.76	1.75	2.13	1.84	1.93	2.18	1.89
Al_2O_3	15.19	15.23	14.45	14.97	14.84	14.59	14.69
Fe_2O_3	9.85	9.35	10.81	9.42	10.57	10.41	9.54
MnO	0.13	0.08	0.13	0.12	0.11	0.13	0.11
MgO	5.26	6.03	7.36	6.53	7.42	7.43	6.99
CaO	8.89	8.81	8.62	6.91	7.87	7.13	7.69
Na_2O	1.01	3.65	3.37	3.55	2.22	3.22	3.14
K_2O	5.15	1.80	2.25	2.35	3.47	2.83	2.51
P_2O_5	0.58	0.40	0.46	0.54	0.40	0.47	0.59
LOI	4.30	3.86	2.21	3.39	3.68	2.18	2.77
Total	99.53	99.86	99.31	99.17	99.44	99.42	99.19
Mg#	*0.51*	*0.56*	*0.57*	*0.58*	*0.58*	*0.59*	*0.59*
Ba (ppm)	360	550	486	698	415	568	834
Cr	114	147	163	124	177	156	113
Hf	5.93	6.35	5.76	5.86	4.81	6.12	6.13
Nb	50.4	49.7	47.7	46.8	40.4	47.5	49.5
Ni	83	94	138	105	147	133	100
Pb	1.8	2.4	2.9	1.9	2.1	3.5	2.1
Rb	25.3	19.6	46.1	27.1	42.5	54.2	30.0
Sr	197	402	471	541	440	741	622
Ta	3.15	3.10	2.98	2.93	2.52	2.97	3.10
Th	4.62	4.50	3.98	4.59	3.97	4.07	4.85
U	0.89	0.94	1.23	0.90	1.24	1.71	1.13
V	120	137	173	125	151	167	128
Y	15.6	17.8	19.6	17.5	18.0	19.5	17.1
Zr	242	263	218	237	177	229	247
La	31.7	34.4	30.1	32.4	27.2	30.6	32.0
Ce	66.5	69.7	61.0	66.5	54.9	62.2	67.9
Pr	8.06	8.86	7.81	8.42	6.91	7.91	8.72
Nd	32.8	37.1	32.4	34.2	27.3	32.8	35.4
Sm	7.04	7.79	7.20	7.38	6.15	7.47	7.64
Eu	2.17	2.35	2.34	2.24	2.00	2.36	2.23
Gd	5.93	6.59	6.69	6.24	5.70	6.65	6.36
Tb	0.87	0.90	1.01	0.90	0.78	1.01	0.90
Dy	4.13	4.46	4.91	4.14	4.05	4.95	4.54
Ho	0.68	0.72	0.84	0.71	0.75	0.86	0.71
Er	1.42	1.54	1.98	1.39	1.82	2.01	1.32
Tm	0.16	0.20	0.28	0.19	0.24	0.27	0.17
Yb	0.96	1.19	1.51	1.12	1.25	1.57	0.96
Lu	0.13	0.16	0.21	0.14	0.18	0.21	0.14

LOI = Ignition loss; #Mg = MgO/(MgO+FeO*) mol

SEIP alkaline basalts and in SCS lamprophyres, although the HREE content of the Cerro Prieto rocks are lower than those recorded in the other magmatic occurrences. A plausible explanation is that the Cerro Prieto magmas generated from an extremely metasomatized (i.e. LREE enriched) mantle source, in the presence of HREE-bearing phases, such as garnet.

Mantle-normalized incompatible trace element data for the Cerro Prieto lamprophyres are compared with the most related rock types in Fig. 10. These lamprophyres display patterns very similar to the average values of OIB (Sun & McDonough, 1989), which are typical of intra-plate alkali-basaltic magmas deriving from deep mantle sources with negligible crustal contribution. They differ from the MSZ Upper Triassic basalts despite their spatial and temporal coexistence and show more analogies with the SCS phlogopite lamprophyres (Fig. 10). In fact, the Cerro Prieto and SCS lamprophyres do not show negative anomalies in Nb-Ta or a positive anomaly in Pb, which are proxies of interaction with continental crust components, via subduction or shallow level assimilation processes, while the MSZ Triassic basalts show evidence of crustal assimilation (Puga, 1988; Puga and Portutal Ferreira, 1989; Morata et al., 1997). Moreover, the high Ce/Pb and Nb/U in the Cerro Prieto lamprophyres, are similar to OIB average values (Fig. 10 and Table 5A) confirming derivation from "enriched" (i.e. metasomatized) mantle sources with negligible crustal contributions. Finally, the lower Yb and Y content in Cerro Prieto lamprophyres, compared with the other magmatic provinces, indicates their deeper origin from a garnet-bearing mantle source (Figs 9 and 10).

Initial Sr and Nd isotope ratios were calculated to 217 M.a., according to $^{40}Ar/^{39}Ar$ radiometric data (on phlogopite) discussed in the following section, using the

TABLE 5 B | **Averange values of whole-rock analyses of Cerro Prieto lamprophyres and other magmatic rocks used for comparison in the text. The type of rocks, number of analyzed samples and analyses provenance are referred in the caption.**

Nº	1	2	3	4	5	6	7	8	9
SiO_2 (wt%)	48.35	49.21	52.45	43.66	48.62	44.50	44.64	47.90	54.99
TiO_2	1.93	1.77	1.40	1.66	1.74	3.04	3.49	1.88	1.41
Al_2O_3	14.85	14.32	14.31	17.37	17.10	15.26	15.95	12.25	10.87
Fe_2O_3	9.99	10.68	11.57	8.01	7.66	11.34	12.11	10.12	6.42
MnO	0.12	0.14	0.18	0.13	0.07	0.16	0.14	0.16	0.08
MgO	6.72	6.31	5.41	4.35	2.41	6.57	5.96	10.38	11.65
CaO	7.99	9.94	8.69	10.20	9.14	8.25	6.82	11.45	5.20
Na_2O	2.88	2.45	3.02	3.02	2.73	2.76	2.82	3.14	1.26
K_2O	2.91	1.22	1.21	2.36	3.48	3.38	3.75	0.92	6.97
P_2O_5	0.49	0.25	0.17	0.25	0.34	0.61	0.66	0.55	0.92
LOI	3.20	3.05	1.59	9.62	6.14	4.08	3.79	0.99	3.35
Total	99.42	99.32	99.99	100.62	99.42	99.94	100.09	99.71	100.28
Mg#	*0.57*	*0.54*	*0.48*	*0.49*	*0.37*	*0.53*	*0.49*	*0.67*	*0.77*
Ba (ppm)	559	261	361	162	260	1212	1719	670	1842
Cr	142	205	166	156	262	167	132	573	572
Hf	5.8	3.79	3.80	3.18	3.58	6.02	6.73	4.69	20.1
Nb	47	22.8	12.4	15.7	19.2	95.9	95.8	56.9	46.2
Ni	114	135	53	48	165	75	50	186	458
Pb	2.4	1.6	8.0		4.1	5.7	5.9	9.1	142
Rb	35	28.8	34.6	23.5	39.8	120	114	18.9	507
Sr	488	294	324	500	390	959	842	618	586
Ta	2.96	1.42	1.00	0.98	1.20	6.18	7.61	3.41	3.23
Th	4.37	2.67	3.20	1.90	3.02	5.50	5.74	17.3	106
U	1.15	1.03	0.75	1.10	0.71	1.17	1.47	3.66	24.2
V	143	173	305	192		287		234	113
Y	17.9	22.6	23.8	18.8	23.4	28.0	45.4	23.2	29.2
Zr	230	143	122	125	153	276	315	197	623
La	31.2	15.7	13.9	12.93	15.3	46.0	63.2	44.6	92
Ce	64.1	31.1	29.4	24.80	31.8	96.0	115	83.0	253
Pr	8.10	4.07	3.84	3.05	4.21	11.0	-	9.91	46.2
Nd	33.1	17.5	17.4	13.87	17.6	44.7	63.7	40.3	155
Sm	7.24	4.45	4.12	3.38	4.31	8.15	12.2	7.32	28.4
Eu	2.24	1.52	1.39	1.22	1.38	2.58	3.54	2.16	4.59
Gd	6.31	4.94	4.54	3.60	4.38	6.99	10.6	6.56	20.3
Tb	0.91	0.79	0.76	0.60	0.71	1.00	-	0.88	1.80
Dy	4.45	4.46	4.92	3.70	4.39	5.38	8.33	4.55	7.11
Ho	0.75	0.86	0.99	0.78	0.88	-	-	0.85	1.03
Er	1.64	2.17	2.82	2.20	2.31	-	4.09	1.89	2.30
Tm	0.21	0.31	0.42	0.32	0.33	-	-	0.30	0.31
Yb	1.22	1.91	2.52	1.97	1.98	2.07	3.68	1.67	2.05
Lu	0.17	0.27	0.39	0.30	0.28	0.32	0.55	0.25	0.28

nº 1 = Cerro Prieto lamprophyres (7 samples, this study); **nº 2** = MSZ dolerites (2 samples, this study); **nº 3** = MSZ Triassic basalts (5 samples, Morata, 1993 & Morata et al., 1997); **nº 4** = MSZ Jurassic basalts (6 samples, Puga et al, 1989; Morata, 1993); **nº 5** = MSZ Cretaceous basalts (3 samples, this study); **nº 6** = SCS camptonitic lamprophyres (7 samples, Perini et al., 2004); **nº 7** = SCS phlogopite-lamprophyres (2 samples, Villaseca et al., 2004); **nº 8** = SEIP alkali-basalts (2 samples, Turner et al., 1999) and **nº 9** = SEIP lamproites (3 samples, Benito et al., 1999 & 2 samples, this study). See data base for this table in Table 1 of the electronic supplement

Sr, Rb, Nd and Sm contents determined by ICP-MS. Time-corrected $^{87}Sr/^{86}Sr$ and $^{143}Nd/^{144}Nd$ isotopes for the Cerro Prieto lamprophyres range from 0.705239 to 0.705803 and 0.512592 to 0.512662, respectively, with a restricted range in εNdi (+4.6 to +5.9) (Table 6 and Fig. 11). These data, plotted in the εNd_i vs $(^{87}Sr/^{86}Sr)_i$ diagram of Fig. 11, reveal a displacement from the MORB-OIB mantle array (Zindler and Hart, 1986; Hoffmann, 1997). Considering that the Sr and Nd content of these lamprophyres is higher than that of most crustal rocks and sediments (Taylor and McLennan, 1985) we conclude that the isotopic composition of the related magmas was nearly immune

TABLE 6 | **Sr and Nd concentrations (ppm) and isotope data of Cerro Prieto lamprophyres.**

Nº	Label	Rb(ppm)	Sr(ppm)	$^{87}Rb/^{86}Sr$	$^{87}Sr/^{86}Sr$	error*	Sm (ppm)	Nd (ppm)	$^{147}Sm/^{144}Nd$	$^{143}Nd/^{144}Nd$	error*
1	3.32 CP	25.3	197	0.3725	0.706377	0.005	7.04	32.8	0.1299	0.512811	0.004
2	14.21 CP	42.5	440	0.2795	0.706391	0.004	6.15	27.3	0.1361	0.512816	0.005
3	PIR-PR-1	20.3	386	0.1519	0.706065	0.005	7.75	36.1	0.1298	0.512846	0.003
4	Pr-Px	46.1	471	0.2830	0.706112	0.002	7.20	32.4	0.1342	0.512783	0.002
5	Pr-Pz-6	54.2	741	0.2114	0.706455	0.003	7.47	32.8	0.1378	0.512804	0.002

error* = Instrumental error expressed as 2σ in %

to shallow level crustal contamination, thus reflecting a mantle fingerprint. This is supported by the above mentioned trace element ratios, as well as by the relative constancy of the obtained Sr-Nd isotopic ratio that depict a restricted compositional range without significant outliers. This, in turn, implies that the Cerro Prieto magmas were formed from a highly metasomatized sub-continental lithospheric mantle, possibly preserving phlogopite-bearing domains characterized by a long-term radiogenic ingrowth that developed higher $^{87}Sr/^{86}Sr$ values than those typically recorded in the sub-oceanic mantle.

On the contrary, the other rock types considered in this study show isotope ratios which are more compatible with the involvement of crustal components in their petrogenesis. Among them, the Cerro Prieto isotopic fingerprint seems relatively more similar to the SCS lamprophyres that show $^{87}Sr/^{86}Sr_i$ from 0.70473 to 0.7049 and εNd_i from +1.2 to -1 (Villaseca et al., 2004), than to the MSZ basaltic rocks characterized by $^{87}Sr/^{86}Sri$ = 0.7040 - 0.70475 and εNd_i from +2.5 to -0.7 (unpublished authors data), and is totally different from the SEIP lamproites showing $^{87}Sr/^{86}Sr_i$ up to 0.7221 and εNd_i down to -12 (Benito et al., 1999; Prelevic et al., 2008; Conticelli et al., 2009). Moreover the moderate alteration process shown by the Cerro Prieto lamprophyres, mainly consisting in the chloritization of olivine, seems not to be the cause for the $^{87}Sr/^{86}Sr$ increase, because the latter is not directly related with the L.O.I. increase of the analysed rocks (Tables 5a and 6).

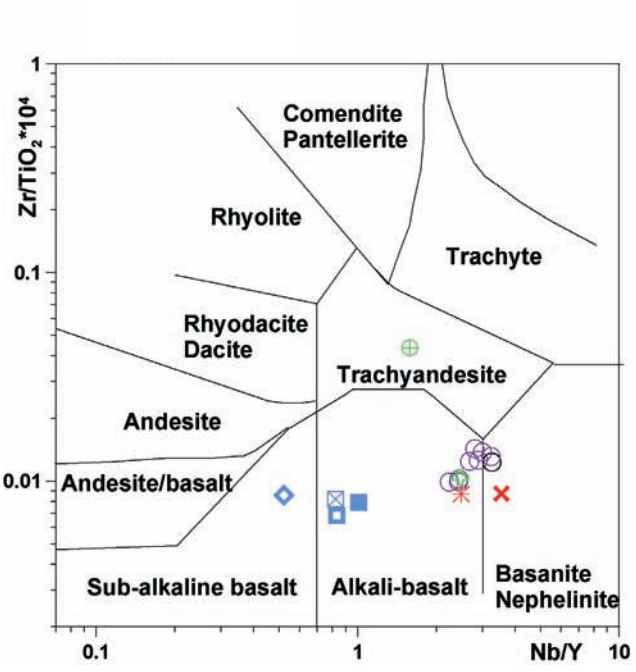

FIGURE 7 | **Zr/TiO_2 vs. Nb/Y diagram after Winchester and Floyd (1977) for Cerro Prieto lamprophyres and related rocks. Key for symbols: circle: Cerro Prieto lamprophyres; filled square: MSZ dolerites; open diamond: MSZ Triassic basalts; open square: MSZ Jurassic basalts; X-shaped cross into square: MSZ Cretaceous basalts; X-shaped cross: SCS Lamprophyres; star: SCS phlogopite lamprophyres; empty cross: SEIP alkali-basalts; cross into circle: SEIP lamproites.**

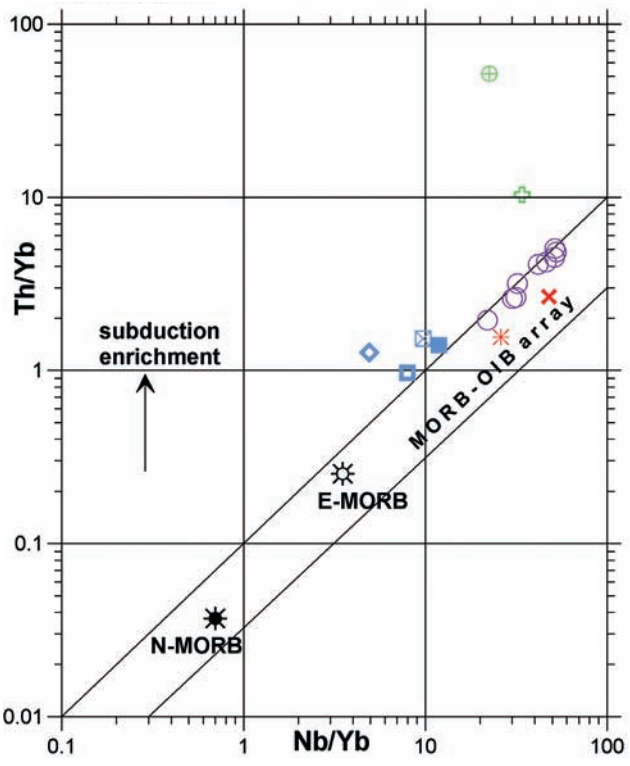

FIGURE 8 | **Th/Yb vs. Nb/Yb plot of the Cerro Prieto lamprophyres and related rocks, in comparison with the MORB-OIB array (Pearce, 1982). Same symbols as in figure 7.**

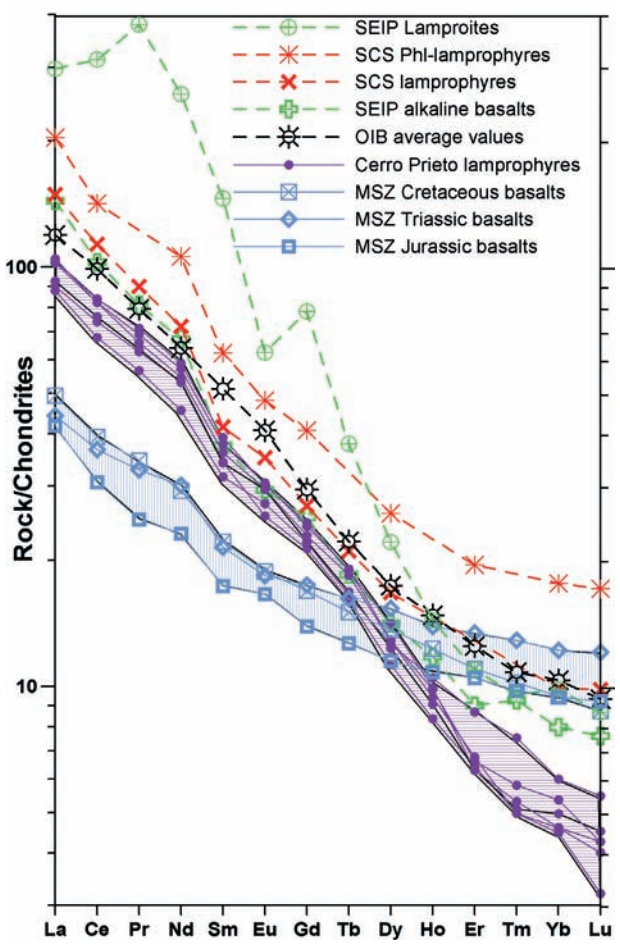

FIGURE 9 | **Chondrite-normalized REE diagram showing that the Cerro Prieto lamprophyre (grey band) have steeper patterns than those of the MSZ magmatism (vertical ruled band) and also than the majority of the other compared rock types. Normalizing values according to Boynton (1984).**

RADIOMETRIC DATING

The phlogopite yielded a spectrum with individual step ages ranging from 211.9 Ma to 225.3 Ma, and plateau calculation provided a weighted age of 217.5 +/- 2.5 Ma (2s) (Fig. 12A). Isochron treatment of the data (Fig. 12B) revealed a simple mixture of modern air argon and radiogenic argon; no excess argon was found as the non-radiogenic intercepts were indistinguishable from atmosphere. The radiogenic intercept age is, within the uncertainty, identical to the plateau age result 216.14 ± 3.90 Ma see Table II in APPENDIX at the electronic version (www.geologica-acta.com).

The groundmass experiment yielded a disturbed spectrum with ages scattered between 160 and 130 Ma in the first three quarters of the gas release, and ages decrease (down to ca 90 Ma) in the final quarter. No plateau was found but the average age is 126.18 ± 10.45 Ma (Fig. 12C), and no good regression was found for the normal isochron (Fig. 12D); extrapolation back to the atmospheric intercept gives an age of 139 ± 11 Ma which is within the uncertainty of the total fusion age 134.7 ± 0.8 Ma see Table III in the APPENDIX at the electronic version.

The $^{40}Ar/^{39}Ar$ dating of 217 ± 2.5 Ma for the phlogopite mineral separates seems to be the most probable age for the emplacement of the Cerro Prieto lamprophyric magmas. Younger radiometric ages for the groundmass, ranging from 160 to 90 Ma, must probably represent rejuvenation ages due to Ar loss caused by the alpine compressive period which started during the Upper Cretaceous and affected the whole Betic Cordilleras inducing high pressure metamorphism (Puga, 1980; Puga et al., 2002, 2004, 2005).

DISCUSSION

Peculiarities of the Cerro Prieto lamprophyres

The Cerro Prieto lamprophyres are difficult to classify following the classic schemes of Le Maitre et al (1989) and Rock et al. (1991), because their modal similitude with a calc-alkaline "minette" contrasts to the alkalinity of their magmas. This rare lamprophyre type must be termed "alkali minette" following the current IUGS recommendations. The uncommon coexistence of olivine, diopside, alkali-feldspar, phlogopite and carbonate implies that the relative magma was under-saturated in silica, rich in potassium as well as in H_2O-CO_2 fluids, thus deriving from highly metasomatized mantle sources.

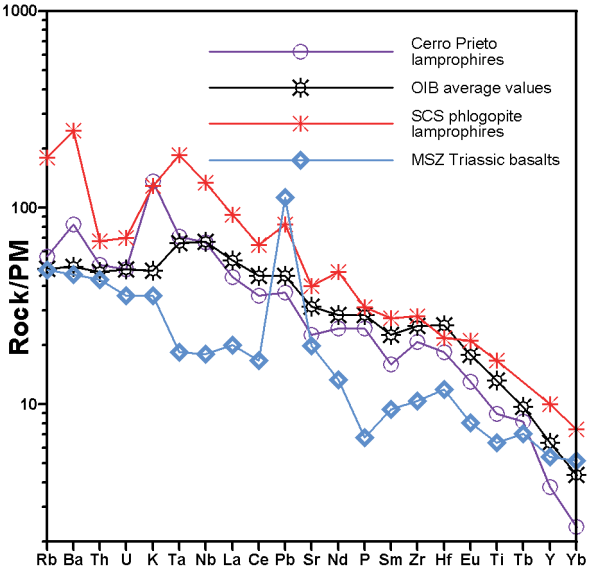

FIGURE 10 | **Primitive mantle-normalized incompatible elements diagram for the Cerro Prieto lamprophyres and the most related rocks. The best match of the average pattern of these lamprophyres is provided by OIB average values in Sun and McDonough (1989).**

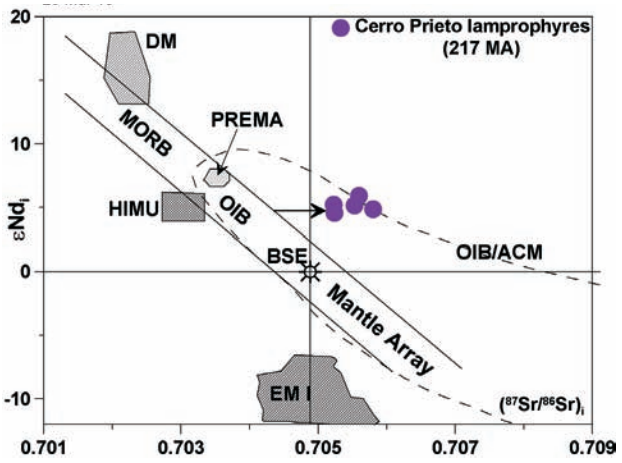

FIGURE 11 | **εNd_i vs. $^{87}Sr/^{86}Sr_i$ isotope correlation diagram for the Cerro Prieto lamprophyres, with initial isotopic ratios calculated at 217 Ma. The principal mantle reservoirs after Zindler and Hart (1986) are also shown: DM: depleted mantle; MORB: mid-ocean ridge basalts; OIB: oceanic islands basalts; PREMA: prevalent mantle; HIMU: high U/Pb mantle; BSE: bulk silicate Earth; EMI: enriched mantle.**

Lamprophyric rocks characterized by a similar mineral paragenesis were described by Vaniman et al. (1985) from rare dykes and subvolcanic bodies at Buell Park (Arizona), which form part of the mid-Tertiary Navajo volcanic Field in the Colorado Plateau. These lamprophyres, named mafic minette (or mica-lamprophyre) by Esperança and Holloway (1987), contain olivine, diopside and Ti-rich phlogopite phenocrysts in a groundmass composed of sanidine, diopside, biotite and titanomagnetite. These authors reported experimental evidences suggesting that similar magmas are obtained from metasomatized (hydrous) garnet-bearing peridotite sources, at pressure ≥ 20 kbar, under $fO_2 \geq$ QFM (quartz-fayalite-magnetite buffers).

The Cerro Prieto lamprophyres are the only known occurrence of this rock type in the Subbetic Zone and all along the Betic Cordilleras. They are different from: a) the MSZ basaltic rocks erupted in the area from the Upper Triassic to the Upper Cretaceous and b) the Neogene SEIP alkali-basalt and lamproitic magmas. In this light, the Cerro Prieto lamprophyres are mineralogically and chemically more similar to the SCS Permian alkaline lamprophyres described by Villaseca et al. (2004).

Age constraints on the emplacement of the Cerro Prieto lamprophyres

The $^{40}Ar/^{39}Ar$ dating carried out on a phlogopite separate from the Cerro Prieto lamprophyres indicates an age of ca 217Ma. The tholeiitic volcanism in the Subbetic Zone has been dated by K/Ar to apparent ages not older than 187 Ma (Puga et al., 1988, Portugal Ferreira et al, 1995), for volcanic rocks interlayered among Upper Triassic sediments with Keuper facies (Morata, 1993). This radiometric rejuvenation compared with the geological age, together with the great dispersion of K/Ar ages obtained even for the same outcrop, has been interpreted as Ar loss during the metamorphism that affected these rocks in the prehnite-pumpellyite to actinolite-pumpellyite facies conditions (Puga et al., 1983, 1988, 2004; Portugal Ferreira et al., 1995). Similar alkaline lamprophyres from the SCS, show ages ranging from the Lower Permian (Bea et al. 1999) or the Late Permian (Scarrow et al., 2006), up to the Upper Triassic (Portugal Ferreira and Regencio, 1979).

According to the new ages presented for the Cerro Prieto lamprophyres, they were emplaced in the Subbetic Zone slightly before or overlapping the beginning of the Upper Triassic tholeiitic magmatic phase, that was followed by the transitional-alkaline magmatism (Figs. 1 and 7). The latter was related to the activation of a system of ENE-WSW oriented lithospheric faults affecting the Middle Subbetic Zone, which triggered the Jurassic and Cretaceous volcanism, together with some subvolcanic basic stocks intruded into Triassic sediments (Comas et al., 1986; Puga et al., 1989; Morata et al., 1997). Although the lamprophyric and tholeiitic magmatism of the Subbetic Zone nearly coincide in time, their petrological and geochemical differences (Figs. 7 to 11), show that they were generated from different mantle sources.

P-T condition of magmagenesis and inferences on the mantle sources

The geochemical characteristics of the Cerro Prieto rocks, show that these lamprophyric magmas are mainly trachybasalts with a predominant alkaline character, generated under non-orogenic distensive conditions, from a LILE-enriched OIB mantle source (Figs. 7 to 11). Primordial mantle normalized trace element-patterns of Cerro Prieto lamprophyres closely approach the OIB average values of Sun and Mc Donough (1989) (Figs. 9 and 10). The great enrichment of the lamprophyric magmas in the most incompatible elements, coupled with their very low HREE content (Yb =0.9-1.6) (Table 5a), suggest that they were generated by low melting degrees (<10%) of a deep, garnet-bearing lherzolite source.

The Putirka (2008) thermobarometer applied to the different clinopyroxene types contained in these lamprophyres, indicates a crystallisation pressure ranging from 17 to 4 kbar (Table 4), thus constraining the minimum depth of provenance of these magmas to approximately 50 km. This is deeper than the estimate reported by Orejana et al (2006) for the pyroxenite segregates, which are comagmatic with the SCS lamprophyric magmas. This difference in depth of origin is in accord with the much lower HREE contents of the Cerro Prieto lamprophyres (Figs. 9 and 10), compared to those of the SCS alkaline lamprophyres. Moreover, the

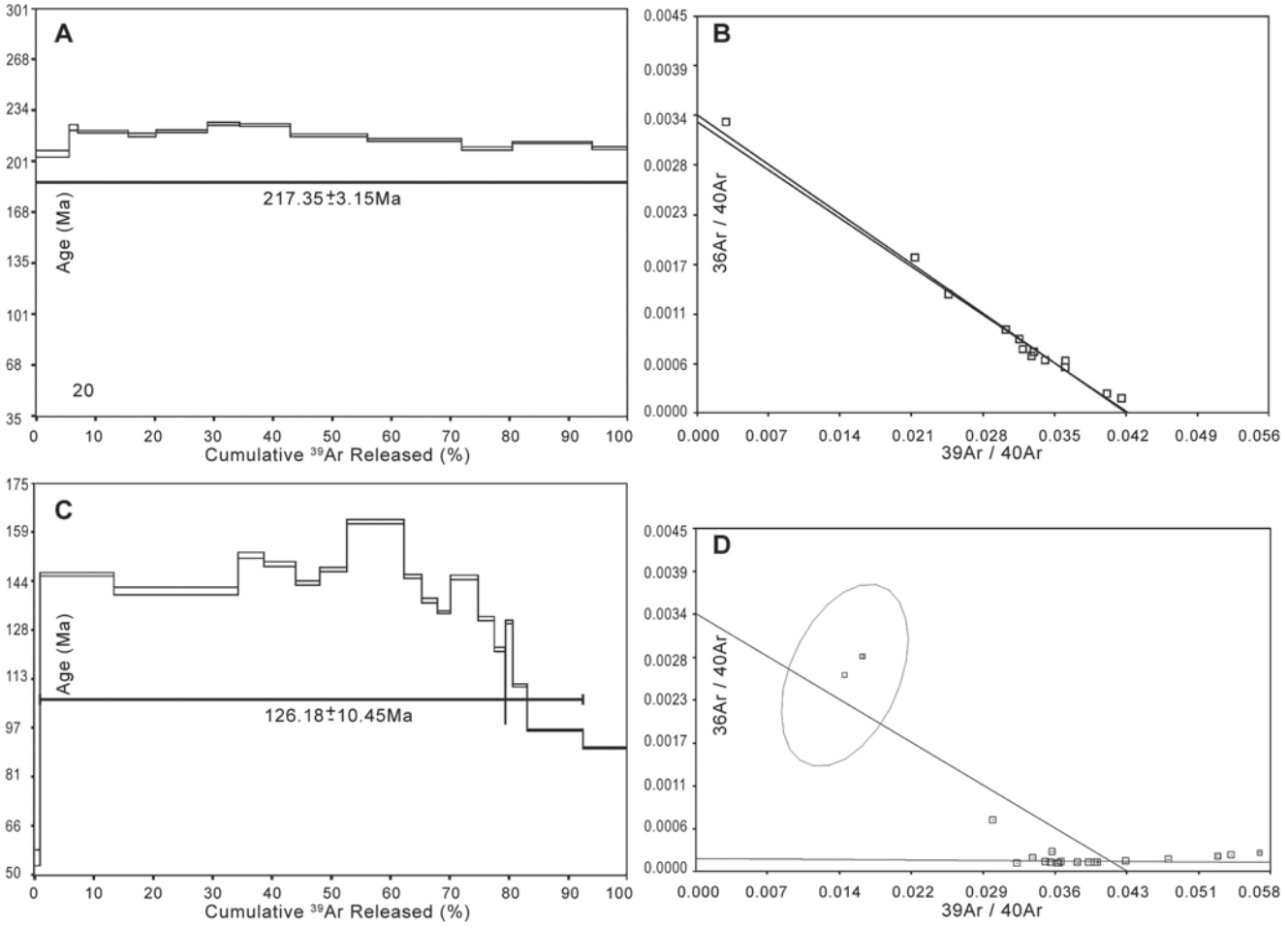

FIGURE 12 | **A, B) Age plateau and inverse isochron obtained by $^{40}Ar/^{39}Ar$ dating of phlogopite from Cerro Prieto lamprophyre; C, D) Age spectrum and inverse isochron for whole-rock groundmass $^{40}Ar/^{39}Ar$ dating of a representative lamprophyric sample of the same locality. See also Tables 2 and 3 of the electronic supplement.**

high depth estimate also agrees with recent experimental evidence indicating that the genesis of similar magmas is related to partial melting of phlogopite-bearing lherzolites within the garnet stability facies (Conceição and Green, 2004 and references therein). The Cerro Prieto mantle source must be related to extremely metasomatized domains, probably containing modal phlogopite, characterized by a high LILE content and high Rb/Sr ratio that ultimately led to $^{87}Sr/^{86}Sr$ compositions enriched with respect to the sub-oceanic mantle array (Fig. 11). Metasomatism of continental lithosphere implies percolation of metasomatic melts rich in volatiles and incompatible elements, into a lithospheric mantle previously depleted by melt extraction (McKenzie and O'Nions, 1995). This conforms to recent studies on mantle xenoliths showing that the Iberian subcontinental lithosphere includes domains characterized by various degrees of metasomatic enrichment (Bianchini et al., 2007 and references therein). The addition of volatiles induces the formation of accessory phases such as phlogopite (and carbonate?) within the lherzolite sources, significantly decreases the solidus temperature, and favours the production of highly alkaline melts, such as those forming the Cerro Prieto lamprophyres (Bianchini et al., 2008)

Geodynamic framework of the Cerro Prieto magmatism

The origin of the SCS alkaline lamprophyres, with OIB signature similar to that of Cerro Prieto, has been interpreted by different authors (Bea et al., 1999; Perini et al., 2004; Villaseca et al., 2004, Orejana et al., 2006; Scarrow et al., 2006) as related to a post-Hercynian lithospheric rifting stage, also recorded in other sectors of the Western European Variscan Orogen. In agreement with this interpretation, we conclude that the Cerro Prieto lamprophyric magmas could have been originated during the same post-Hercynian lithospheric rifting event, which also affected the Southern Iberian Paleomargin represented by the Subbetic Zone of the Betic Cordilleras (Vera, 2001). It is worth noting that the Cerro Prieto lamprophyres represents, as far as we

know, the only magmatic occurrence in the Subbetic Zone corresponding to the initial phase of this post-Hercynian extensional intracontinental magmatism. This magmatism is better represented in the SCS by a network of a hundred of N-S/NNE-SSW subvertical lamprophyre dykes (Bea et al., 1999). The more abundant Upper Triassic to Upper Cretaceous magmatism, which developed all along the Subbetic Zone (Fig.1), was genetically related to the opening of the central part of the Atlantic ocean (Comas et al., 1986; Puga et al., 1989; Morata et al., 1997), and/or by the westward propagation of the Neotethys rift system and subsequent oceanization stage (Dewey et al., 1973; Guerrera et al., 1993; Ziegler, 1993; Vera, 2001; Puga, 2005). Within this distensive to transtensive framework, the uplift of the asthenosphere caused continental breakup and the intrusion of basic magmas at the plate margins, mainly through a network of pre-existing deep late-Hercynian faults (Parga, 1969; Bertrand and Coffrant, 1977; Graziansky et al., 1979).

The mantle source needed to originate the Cerro Prieto lamprophyric magmas was plausibly located in the Iberian sub-continental lithosphere, which includes mantle domains diversely enriched by metasomatism (Bianchini et al., 2007). The more metasomatized mantle portions would be preferentially affected by melting during the initial phase of the post-Hercynian extensional cycle, which generated the Cerro Prieto magma-type in the Subbetic Zone. Subsequently, in relation with the Mesozoic distensive to transtensive regime, the character of the South Iberian Margin magmatism changed from tholeiitic to slightly sodic-alkaline series. These magmas derived from shallower lithospheric mantle sources which were affected by higher melting degrees and they commonly show clear indices of crustal assimilation (Puga, 1987; Puga and Portugal Ferreira, 1989; Puga et al., 1989; Morata et al., 1997).

CONCLUSIONS

The Cerro Prieto subvolcanic body, emplaced ca 217 Ma ago, is formed by lamprophyric rocks that could be classified as “alkali minette”. This represents the only occurrence of lamprophyres in the Subbetic Zone and more in general in the whole Betic Cordilleras.

The lamprophyric magma was generated in intraplate tectonic setting by low degree of partial melting of a lithospheric mantle source. These were equilibrated in the garnet peridotite facies (≥60 km depth) and affected by interaction with metasomatic agents, ultimately leading to modal formation of phlogopite, OIB-type trace element enrichment, and enriched mantle Sr-Nd isotopic composition slightly displaced from the sub-oceanic mantle array.

Magma genesis was plausibly triggered by extensional tectonic activity, marking the onset of a tectono-magmatic cycle that from the post-Hercynian rifting phase progressively evolved, by ascent of the asthenosphere, toward continental breakup and opening of the Atlantic and Neotethys oceans, accompanied by intrusion of basic magmas along their continental margins.

ACKNOWLEDGMENTS

The first author (E.P.) would like to express her gratitude to M. Ruiz Montes co-finder, together with M.A. Díaz Puga, of the first blocks of lamprophyre near of the Vivarena farmhouse, during a research on the historical mines of the Malaga province, and to J.A. Lozano for his field work focussed on finding further vestiges of this type of rock within the Antequera Trias. The authors are also in debt to M. Gonzalez, owner of the Vivarena farmhouse who generously allowed the perforation of a new drilling for sampling “in situ” the not-outcropping at surface lamprophyre body. They are also very grateful to F. Bea, J.L. López Ruiz and C. Villaseca, for their constructive criticism of an early version of the manuscript, so as to the valuable and meticulous revision of the Editor (F. Costa) and the Reviewers (J.M. Cebria and D. Prelevic), which have greatly helped to improve the final version. Some preliminary K/Ar dating of the studied rocks performed by M. Portugal Ferreira and R. Macedo are also acknowledged, so as the linguistic revision of the manuscript made by B. Galassi. This research was funded by Projects CGL 2005-24177BTE, CGL2006-06001, and CSD2006-00041, of the Spanish Ministry of Science and Technology, co-financed with FEDER funds, and by Research Group RNM 333 of the Junta de Andalucía (Spain).

REFERENCES

Aguirre, L., Morata, D., Puga, E., Baronet, A., Beiersdorfer, R.E., 1995. Chemistry and crystal characteristics of pumpellyite in a metadolerite from the Archidona region, Subbetic Cordillera, Spain. Geological Society of America, 296(Special Paper), 171-181.

Bea, F., Montero, P., Molina, J.F., 1999. Mafic precursors, peraluminous granitoids, and late lamprophyres in the Avila batholith; a model for the generation of Variscan batholiths in Iberia. Journal of Geology, 107, 399-419.

Benito, R., López-Ruiz, J., Cebriá, J.M., Hertogen, J., Doblas, M., Oyarzum, R., Demaiffe, D., 1999. Sr and O isotope constraints on source and crustal contamination in the high-K calc-alkaline and shoshonitic neogene volcanic rocks of SE Spain. Lithos, 46, 773-882.

Bertrand, H., Coffrant, D., 1977. Geochemistry of tholeiites from North-East American Margin: Correlation with Morocco. A statistical approach. Contribution to Mineralogy and Petrology, 63, 65-74.

Bianchini, G., Beccaluva, L., Bonadiman, C., Nowell, G., Pearson, G., Siena, F., Wilson, M., 2007. Evidence of distinct depletion

and metasomatic processes in harzburgite-lherzolite mantle xenoliths from the Iberian lithosphere (Olot, NE Spain). Lithos, 94, 25-45.

Bianchini, G., Beccaluva, L., Siena, F., 2008. Post-collisional and intraplate Cenozoic volcanism in the rifted Apennines/ Adriatic domain. Lithos, 101, 125-140.

Bohoyo, F., Galindo-Zaldivar, J., Serrano, I., 2000. Main features of the basic rock bodies of the Archidona Region derived from geophysical data (External Zones, Betic Cordillera). Earth and Planetary Science Letters, 330, 667-674.

Boynton, W.V., 1984. Geochemistry of rare earth elements: meteorite studies. In: Henderson, P. (ed.). Rare earth element geochemistry. Amsterdam, Elsevier, 63-114.

Comas, M.C., Puga, E., Bargossi, G.M., Morten, L., Rossi, P.L., 1986. Paleogeography, sedimentation and volcanism of the Central Subbetic Zone, Betic Cordilleras, Southeastern Spain. Neües Jahrbuch fur Geology and Paläntology, 186, 385-402.

Conceição, R.V., Green, D.H., 2004. Derivation of potassic (shoshonitic) magmas by decompression melting of phlogopite+pargasite lherzolite. Lithos, 72, 209-229.

Conticelli, S., Guarnieri, L., Farinelli, A., Mattei, M., Avanzinelli, R., Bianchini, G., Boari, E., Tommasinik, S., Tiepolo, M., Prelević, D., Venturelli, G., 2009. Trace elements and Sr-Nd-Pb isotopes of K-rich, shoshonitic, and calc-alkaline magmatism of the Western Mediterranean Region: Genesis of ultrapotassic to calc-alkaline magmatic associations in a post-collisional geodynamic setting. Lithos, 107, 68-92.

Deer, W.A., Howie, R.A., Zussman, J., 1992. An Introduction to the Rock-forming Minerals. London, Longman Group UK Limited, 2nd edition, 696pp.

Dewey, J.F., Pitman III, W.C., Ryan, W.B.F., Bonnin, J., 1973. Plate tectonics and the evolution of the Alpine System. Geological Society American Bulletin, 84, 3137-3180.

Droop, G.T.R., 1987. A general equation for estimating Fe^{3+} concentrations in ferromagnesian silicates and oxides from microprobe analyses using stoichiometric criteria. Mineralogical Magazine, 51, 431-435.

Esperança, S., Holloway, R., 1987. On the origin of some mica-lamprophyres: experimental evidence from a mafic minette. Contribution to Mineralogy and Petrology, 95, 207-216.

Govindaraju, K., 1994. Compilation of working values and sample description for 383 geostandards. Geostandards Newsletter, 18, 1-158.

Graciansky, P.Ch., Bourbon, M., Charpal, O., Chenet, P.Y., Lemoine, M. 1979. Genèse et évolution comaprées de deux marges continentals passives: marge ibérique de l´Océan Atlantique et marge européenne de la Téthys dans les Alpes occidentales. Bulletin de la Societé Géologique de France, 7/ XXI-5, 663-674.

Guerrera, F., Martin-Algarra, A., Perrone, V., 1993. Late Oligocene-Miocene syn-/-late-orogenic succesions in Western and Central Mediterranean Chains from the Betic Cordillera to the Southern Apennines. Terra Nova, 5(6), 525-544.

Hoffman, A.V., 1997. Mantle geochemistry: The message from oceanic volcanism. Nature, 385, 219-229.

Kretz, R., 1983. Symbols for rock-forming minerals. American Mineralogist, 68, 277-279.

Le Bas, M.J., Le Maitre, R.W., Streckeisen, A., Zanettin, B., 1986. A chemical classification of volcanic rocks based on the total alkali-silica diagram. Journal of Petrology, 27, 745-750.

Le Maitre, R.W., Bateman, P., Dudek, A., Keller, J., Le Bas, M.J., Sabine, P.A., Schmid, R., Sorensen, H., Streckeisen, A., Woolley, A.R., Zanettin, B., 1989. A classification of igneous rocks and glossary of terms. Oxford, Blackwell Scientific Publications, 196pp.

McKenzie, D., O'nions, K.R., 1995. The source regions of ocean island basalts, Journal of Petrology, 36, 133-159.

Mercier, J-C.C., Nicolas, A., 1975. Textures and fabrics of Upper-Mantle peridotites as illustrated by xenoliths from basalts. Journal of Petrology, 16, 454-487.

Molina, J.M., Vera, J.A., Gea, G.A., 1998. Vulcanismo submarino del Santoniense en el Subbético: datación con nannofósiles (Formación Capas Rojas, Alamedilla, Provincia de Granada). Estudios Geológicos, 54, 191-197.

Morata, D., 1993. Petrología y geoquímica de las ofitas de las Zonas Externas de las Cordilleras Béticas. Doctoral Thesis. Granada University, 432pp.

Morata, D., Puga, E., Demant, A., Aguirre, L., 1997. Geochemistry and tectonic setting of the Ophites from the External Zones of the Betic Cordilleras (S. Spain). Estudios Geológicos, 53, 107-120.

Morimoto, N., Fabrie, J., Ferguson, A.K., Ginzburg, I.V., Ross, M., Seifert, F.A., Zussman, J., 1988. Nomenclature of pyroxenes. Mineralogical Magazine, 52, 535-550.

Nimis, P., 1995. A clinopyroxene geobarometer for basaltic systems based on crystals-structure modeling. Contribution to Mineralogy and Petrology, 121, 115-125.

Orejana, D., Villaseca, C., Paterson, B.A., 2006. Geochemistry of pyroxenitic and hornblenditic xenoliths in alkaline lamprophyres from the Spanish Central System. Lithos, 86, 167-196.

Parga, J.R., 1969. Sistemas de fracturas tardihercínicas del Macizo Hespérico. Trabajos del Laboratorio Geológico de Lage, 37, 1-15.

Pearce, J.A., 1982. Trace element characteristics of lavas from destructive plate boundaries. In: Thorpe, R.S. (eds.). Andesites. New York, John Wiley and Sons, 525-548.

Pedley, R.C., Bubsby, J.P., Dabek, Z.K., 1993. GRAVMAG vl.5 USER MANUAL Interactive 2.5D gravity and magnetic modelling. Technical Report WK/93/26/R Regional Geophysics Series, British Geological Survey, 77pp.

Perini, G., Cebriá, J.M., López-Ruiz, J., Doblas, M., 2004. Carboniferous-Permian mafic magmatism in the Variscan belt of Spain and France: implications for mantle sources. In: Wilson, M., Neumann, E.R., Davies, G.R., Timmerman, M.J., Heeremans, M., Larsen, B.T. (eds.). Permo-Carboniferous Magmatism and Rifting in Europe. Geological Society of London, 223, 415-438.

Piccardo, G.B., Müntener, O., Zanetti, A., Romairone, A., Bruzzone, S., Poggi, E., Spagnolo, G., 2004. The Lanzo

South peridotite: Melt/peridotite interaction in the mantle lithosphere of the Jurassic Ligurian Tethys. Ofioliti, 29, 37-62.

Pineda Velasco, A., 1990. Mapa Geológico de España 1:50.000. Archidona, Instituto Geológico y Minero de España, hoja nº 1024.

Portugal Ferreria, M., Regencio, C.A., 1979. Actividade magmatica durante o Mesozoico: l-achega para a dataçao K-Ar das rochas filonianas básicas intrusivas da zona Centro-Ibérica (Portugal). Memorias e Publicacioes Laboratorio Mineralogico Geologico Universidade de Coimbra, 87, 29-49.

Portugal Ferreira, M., Morata, D., Puga, E., Demant, A., Aguirre, L., 1995. Evolución geoquímica y temporal del magmatismo básico mesozoico en las zonas externas de las Cordilleras Béticas. Estudios Geológicos, 51, 109-118.

Prelevic, D., Foley, S.F., Romer, R., Conticelli, S., 2008. Mediterranean Tertiary lamproites derived from multiple source components in postcollisional geodynamics. Geochimica et Cosmochimica Acta, 72, 2125-2156.

Puga, E., 1980. Hypothèse sur la genèse des magmatismes calcoalcalins intra-orogénique et post-orogénique alpins, dans les Cordillères Bétiques. Bulletin de la Société Géologique de France, 7, 243-250.

Puga, E., 1987. Enclaves de micaschistes à silicates d´alumine dans les roches volcaniques basiques mèsozoiques de la Cordillère Subbètique: premiers tèmoins d´un socle, non affleurant, dans les Zones Betiques Externes (Spagne du Sud). Comptes Rendus Academie des Sciences, 305(II), 1503-1506.

Puga, E., 2005. A reappraisal of the Betic Ophiolitic Association: The westernmost relic of the Alpine Tethys Ocean). In: Finetti, I.R. (ed.). Deep Seismic Exploration of the Central Mediterranean and Italy. Italy, University of Trieste, Elsevier, Crosta Profonda (CROP), 1, 665-704.

Puga, E., Morten, L., Bondi, M., Bargossi, J.M., Ruiz Cruz, M.D., Díaz de Federico, A., 1983. Metamorphosed "ophites" from Archidona region, Subbetic Zone, Spain. Estudios Geológicos, 39, 307-317.

Puga, E., Van de Fliert, J.R., Torres Roldan, R.L., Sanz de Galdeano, C., 1988. Attempts of whole-rock K/Ar dating of Mesozoic volcanic and hypabissal igneous rocks from the Central Subbetic (Southern Spain): A case of differential Argon loss related to very low-grade metamorphism. Estudios Geológicos, 44, 47-59.

Puga, E., Portugal Ferreira, M., 1989. The recrystallization and partial melting of xenoliths of pelitic rocks and their bearing on the contaminated basalts (Subbetic Zone, Spain). In: Bonin, B., Didier, J., Le Fort, P., Propach, G., Puga, E. Vistelius, A.B. (eds.). Magma-Crust interactions and evolution. Athens, Theophrastus Publications, 115-159.

Puga, E., Portugal Ferreira, M., Díaz de Federico, A., Bargossi, G.M., Morten, L., 1989. The evolution of the magmatism in the external zones of the Betic Cordilleras during the Mesozoic. Geodinamica Acta, 3, 253-266.

Puga, E., Díaz de Federico, A., Nieto, J.M., 2002. Tectono-stratigraphic subdivision and petrological characterisation of the deepest complexes of the Betic Zone: a review. Geodinámica Acta, 15, 23-43.

Puga, E., Morata, D., Díaz de Federico, A., 2004. Magmatísmo Mesozoico y metamorfismo de muy bajo grado de las Zonas Externas Béticas. In: Vera, J.A. (ed.). Geología de España. Madrid, Sociedad Geográfica de España-Instituto Geológico y Minero de España, 386-387.

Puga, E., Fanning, C.M., Nieto, J.M., Díaz De Federico, A., 2005. New recrystallisation textures in zircons generated by ocean-floor and eclogite facies metamorphism: a cathodoluminescence and U-Pb SHRIMP study with constraints from REE elements. Canadian Mineralogist, 42(Carmichael Volume), 183-202.

Putirka, K., 2008. Thermometers and Barometers for Volcanic Systems. In: Putirka, K., Tepley, F. (eds.). Minerals, Inclusions and Volcanic Processes. Reviews in Mineralogy and Geochemistry, U.S.A., Mineralogical Society of America, 69, 61-120.

Rock, N.M.S., Bowes, D.R., Wright, A.E. (eds.), 1991. Lamprophyres. New York, Blackie and Son, 285pp.

Sanz de Galdeano, C., Lozano, J.A., Puga, E., 2009. El "trías" de Antequera: origen, estructura y posible significado. Revista de la Sociedad Geológica de España, 22(3-4), 111-124.

Scarrow, J.H., Bea, F., Montero, P., Molina, J.F., Vaughan, A.P.M., 2006. A precise late Permian $^{40}Ar/^{39}Ar$ age for Central Iberian camptonitic lamprophyres. Geologica Acta, 4(4), 451-459.

Sun, S.S., McDonough, W.F., 1989. Chemical and isotopic systematics of oceanic basalts; implications for mantle composition and processes. In: Saunders, A.D., Norry, M.J. (eds.). Magmatism in the oceanic basins. Geological Society of London, 42(Special Publication), 313-345.

Taylor, S.R., McLennan, S.M., 1985. The Continental Crust: Its composition and Evolution. Oxford, Blackwell Scientific Publications, 312pp.

Turner, S.P., Platt, J.P., George, R.M.M., Kelley, S.P., Pearson, D.G., Nowell, G.M., 1999. Magmatism associated with orogenic collapse of the Betic-Alboran Domain, SE Spain. Journal of Petrology, 40, 1011-1036.

Vaniman, D., Laughlin, A.W., Gladney, E.S., 1985. Navajo minettes in the Cerro de las Mujeres, New Mexico. Herat Planetary Science Letters, 74, 69-80.

Vera, J.A., 2001. Evolution of the South Iberian Continental Margin. In: Ziegler, P.A., Cavazza, W., Robertson, A.H.F., Crasquin-Soleau, S. (eds.). Peri-Tethyan Rift/Wrench Basins and Passive Margins. París, Mémoire Museum Histoire Naturalle, 186, 109-143.

Villaseca, C., Orejana, D., Pin, C.H., López García, J.A., Andonaegui, P., 2004. Le magmatisme basique hercynien et post-hercynien du Système central espagnol: essai de caractérisation des sources mantelliques. Comptes Rendus Geoscience, 336, 877-888.

Wijbrans, J., Németh, K., Martin, U., Balogh, K., 2007. $^{40}Ar/^{39}Ar$ geochronology of Neogene phreatomagmatic volcanism in the Western Pannonian Basin, Hungary. Journal of Volcanology and Geothermal Research, 164, 193-204.

Winchester, J.A., Floyd, P.A., 1977. Geochemical discrimination of different magma series and their differentiation products using immobile elements. Chemical Geology, 20, 325-343.

Woolley, A.R., Bergman, S.C., Edgar, A.D., Le Bas, M.J., Mitchell, R.H., Rock, N.M.S., Scott Smith, B.H., 1996. Classification of lamprophyres, lamproites, kimberlites, and the kalsilitic, melilitic, and leucitic rocks. Canadian Mineralogist, 34, 175-186.

Ziegler, P.A., 1993. Late Palaeozoic-Early Mesozoic plate reorganization: evolution and demise of the Variscan fold belt. In: Raumer, J.F., Nebauer, F. (eds.). Pre-Mesozoic geology in the Alps. Berlin, Springer Verlag, 203-216.

Zindler, A., Hart, S., 1986. Chemical geodynamics. Annual Reviews Earth Planetary Science, 14, 493-571.

Manuscript received October 2008;
revision accepted April 2009;
published Online January 2010.

APPENDIX

TABLE I | **Data base for Table 5b in the text.**

Rocks	Lamprophyres Cerro Prieto								MSZ Dolerites			MSZ Triassic Basalts						
Symbol	Circle							Filled square				Empty rhomb						
Label	6.43 MATRIZ	6.5 CP	14.21 CP	Pr-Px	Pr-Pz-6	Pir-Pr-1	3.32 CP	**Average**	Pr-Of	15.51 CP	Average	ALCII-6	CEG2-1	ALCII-A8	ALCII-B1	SPA-16	**Average**
SiO_2 (%)	49.55	49.26	46.93	47.52	48.85	48.90	47.41	**48.35**	51.33	47.09	**49.21**	52.79	52.94	52.90	52.0146	51.62	**52.45**
TiO_2	1.84	1.89	1.93	2.13	2.18	1.75	1.76	**1.93**	1.83	1.71	**1.77**	1.13	1.35	2.13	1.1385	1.26	**1.40**
Al_2O_3	14.97	14.69	14.84	14.45	14.59	15.23	15.19	**14.85**	14.89	13.75	**14.32**	14.50	16.58	12.26	14.1273	14.07	**14.31**
Fe_2O_3	9.42	9.54	10.57	10.81	10.41	9.35	9.85	**9.99**	10.92	10.44	**10.68**	10.57	7.83	16.14	11.3355	11.98	**11.57**
MnO	0.12	0.11	0.11	0.13	0.13	0.08	0.13	**0.12**	0.14	0.14	**0.14**	0.15	0.12	0.23	0.1782	0.22	**0.18**
MgO	6.53	6.99	7.42	7.36	7.43	6.03	5.26	**6.72**	5.98	6.64	**6.31**	6.46	4.43	3.49	6.93	5.71	**5.41**
CaO	6.91	7.69	7.87	8.62	7.13	8.81	8.89	**7.99**	8.74	11.14	**9.94**	9.52	7.82	7.87	9.3654	8.88	**8.69**
Na_2O	3.55	3.14	2.22	3.37	3.22	3.65	1.01	**2.88**	2.70	2.19	**2.45**	3.08	4.50	2.53	2.2572	2.72	**3.02**
K_2O	2.35	2.51	3.47	2.25	2.83	1.80	5.15	**2.91**	1.17	1.26	**1.22**	0.66	1.30	1.21	1.5147	1.37	**1.21**
P_2O_5	0.54	0.59	0.40	0.46	0.47	0.40	0.58	**0.49**	0.26	0.25	**0.25**	0.12	0.16	0.26	0.1386	0.16	**0.17**
LOI	3.39	2.77	3.68	2.21	2.18	3.86	4.30	**3.20**	1.35	4.74	**3.05**	1.47	3.39	0.54	0.77	1.77	**1.59**
TOTAL	**99.17**	**99.19**	**99.44**	**99.31**	**99.42**	**99.86**	**99.53**	**99.42**	**99.31**	**99.34**	**99.32**	**100.46**	**100.41**	**99.55**	**99.77**	**99.76**	**99.99**
Mg#=MgO/(MgO+FeO)mol*	*57.86*	*59.20*	*58.17*	*57.42*	*58.57*	*56.09*	*51.40*	*56.96*	*52.03*	*55.75*	*53.89*	*0.55*	*0.53*	*0.30*	*0.55*	*0.49*	*0.48*
Ba (ppm)	698	834	415	486	568	550	360	**559**	332	189	**261**	315	557	375	250	307	**361**
Cr	124	113	177	163	156	147	114	**142**	216	194	**205**	263	183	16	260	110	**166**
Hf	5.86	6.13	4.81	5.76	6.12	6.35	5.93	**5.85**	4.00	3.58	**3.79**	3.00	4.00	6.00	3.00	3.00	**3.80**
Nb	46.8	49.5	40.4	47.7	47.5	49.7	50.4	**47.4**	24.8	20.8	**22.8**	17.0	15.0	14.0	8.0	8.0	**12.4**
Ni	105	100	147	138	133	94	83	**114**	133	137	**135**	65	75	16	65	46	**53**
Pb	1.9	2.1	2.1	2.9	3.5	2.4	1.8	**2.4**	1.3	1.9	**1.6**	<2	8.0	<2	<2	<2	**8.0**
Rb	27	30	43	46	54	20	25	**35**	31	27	**29**	25	37	38	39	34	**35**
Sr	541	622	440	471	741	402	197	**488**	321	267	**294**	200	722	227	262	208	**324**
Ta	2.93	3.10	2.52	2.98	2.97	3.10	3.15	**2.96**	1.55	1.30	**1.42**	<1	<1	1.00	<1	<1	**1.00**
Th	4.59	4.85	3.97	3.98	4.07	4.50	4.62	**4.37**	2.60	2.74	**2.67**	2.00	3.00	5.00	3.00	3.00	**3.20**
U	0.90	1.13	1.24	1.23	1.71	0.94	0.89	**1.15**	0.74	1.31	**1.03**	0.60	<0.5	1.00	0.70	0.70	**0.75**
V	125	128	151	173	167	137	120	**143**	183	164	**173**	293	312	349	283	289	**305**
Y	17.5	17.1	18.0	19.6	19.5	17.8	15.6	**17.9**	23.9	21.3	**22.6**	22.0	15.0	37.0	22.0	23.0	**23.8**
Zr	239	247	200	218	229	263	242	**234**	154	132	**143**	110	114	167	103	117	**122**
La	32.44	31.97	27.23	30.15	30.56	34.43	31.70	**31.21**	16.32	15.06	**15.69**	11.90	11.00	21.70	11.70	13.20	**13.90**
Ce	66.46	67.90	54.88	60.97	62.22	69.73	66.48	**64.09**	32.47	29.71	**31.09**	25.90	25.10	44.20	24.20	27.40	**29.36**
Pr	8.42	8.72	6.91	7.81	7.91	8.86	8.06	**8.10**	4.24	3.90	**4.07**	3.50	3.50	5.80	3.00	3.40	**3.84**
Nd	34.21	35.38	27.34	32.43	32.78	37.13	32.77	**33.15**	18.31	16.66	**17.48**	15.90	15.70	26.50	13.10	15.80	**17.40**
Sm	7.38	7.64	6.15	7.20	7.47	7.79	7.04	**7.24**	4.67	4.24	**4.45**	3.60	4.00	6.10	3.20	3.70	**4.12**
Eu	2.24	2.23	2.00	2.34	2.36	2.35	2.17	**2.24**	1.65	1.39	**1.52**	1.24	1.34	1.94	1.07	1.34	**1.39**
Gd	6.24	6.36	5.70	6.69	6.65	6.59	5.93	**6.31**	5.07	4.81	**4.94**	4.20	4.20	6.80	3.40	4.10	**4.54**
Tb	0.90	0.90	0.78	1.01	1.01	0.90	0.87	**0.91**	0.84	0.75	**0.79**	0.70	0.70	1.10	0.60	0.70	**0.76**
Dy	4.14	4.54	4.05	4.91	4.95	4.46	4.13	**4.45**	4.81	4.11	**4.46**	4.40	4.40	7.10	4.10	4.60	**4.92**
Ho	0.71	0.71	0.75	0.84	0.86	0.72	0.68	**0.75**	0.86	0.86	**0.86**	0.90	0.86	1.45	0.80	0.93	**0.99**
Er	1.39	1.32	1.82	1.98	2.01	1.54	1.42	**1.64**	2.27	2.08	**2.17**	2.40	2.50	4.10	2.40	2.70	**2.82**
Tm	0.19	0.17	0.24	0.28	0.27	0.20	0.16	**0.21**	0.33	0.30	**0.31**	0.40	0.40	0.60	0.30	0.40	**0.42**
Yb	1.12	0.96	1.25	1.51	1.57	1.19	0.96	**1.22**	1.94	1.88	**1.91**	2.30	2.20	3.50	2.30	2.30	**2.52**
Lu	0.14	0.14	0.18	0.21	0.21	0.16	0.13	**0.17**	0.28	0.27	**0.27**	0.35	0.31	0.54	0.36	0.37	**0.39**

TABLE II | **Data Tables and Figures of phlogopite $^{40}Ar/^{39}Ar$ dating from Cerro Prieto lamprophyre.**

Procedure Blanks		^{36}Ar	1σ	^{37}Ar	1σ	^{38}Ar	1σ	^{39}Ar	1σ	^{40}Ar	1σ
06MY495A	4.00 W	0.000108	0.000011	0.000740	0.000013	0.000111	0.000017	0.000175	0.000025	0.019352	0.000441
06MY495B	8.00 W	0.000108	0.000011	0.000740	0.000013	0.000111	0.000017	0.000175	0.000025	0.019352	0.000441
06MY495C	12.00 W	0.000108	0.000011	0.000740	0.000013	0.000111	0.000017	0.000175	0.000025	0.019352	0.000441
06MY495D	16.00 W	0.000108	0.000011	0.000740	0.000013	0.000111	0.000017	0.000175	0.000025	0.019352	0.000441
06MY495E	18.00 W	0.000108	0.000011	0.000740	0.000013	0.000111	0.000017	0.000175	0.000025	0.019352	0.000441
06MY495F	20.00 W	0.000108	0.000011	0.000740	0.000013	0.000111	0.000017	0.000175	0.000025	0.019352	0.000441
06MY495G	22.00 W	0.000108	0.000011	0.000740	0.000013	0.000111	0.000017	0.000175	0.000025	0.019352	0.000441
06MY495H	24.00 W	0.000108	0.000011	0.000740	0.000013	0.000111	0.000017	0.000175	0.000025	0.019352	0.000441
06MY495I	30.00 W	0.000108	0.000011	0.000740	0.000013	0.000111	0.000017	0.000175	0.000025	0.019352	0.000441
06MY495J	35.00 W	0.000108	0.000011	0.000740	0.000013	0.000111	0.000017	0.000175	0.000025	0.019352	0.000441
06MY495K	40.00 W	0.000108	0.000011	0.000740	0.000013	0.000111	0.000017	0.000175	0.000025	0.019352	0.000441
06MY495L	50.00 W	0.000108	0.000011	0.000740	0.000013	0.000111	0.000017	0.000175	0.000025	0.019352	0.000441
06MY495M	60.00 W	0.000108	0.000011	0.000740	0.000013	0.000111	0.000017	0.000175	0.000025	0.019352	0.000441

Intercept Values		^{36}Ar	1σ	r_2		^{37}Ar	1σ	r_2		^{38}Ar	1σ	r_2
06MY495A	4.00 W	0.023857	0.000102	0.9901	LIN # 3	0.001875	0.000029	0.6721	LIN #	0.005040	0.000055	0.9990
06MY495B	8.00 W	0.005845	0.000014	0.9959	LIN # 9	0.001610	0.000008	0.9857	LIN #	0.002331	0.000017	0.9992
06MY495C	12.00 W	0.010885	0.000048	0.9777	LIN # 11	0.004057	0.000027	0.9775	LIN #	0.005537	0.000053	0.9990
06MY495D	16.00 W	0.002387	0.000008	0.9855	LIN # 7 12	0.000904	0.000007	0.9586	LIN #	0.002266	0.000009	0.9998
06MY495E	18.00 W	0.001960	0.000008	0.9776	LIN #	0.000833	0.000006	0.9709	LIN #	0.001393	0.000007	0.9996
06MY495F	20.00 W	0.002048	0.000008	0.9668	LIN # 10	0.000980	0.000007	0.9697	LIN #	0.002266	0.000013	0.9995
06MY495G	22.00 W	0.001434	0.000008	0.9562	LIN # 4	0.000604	0.000005	0.9550	LIN #	0.001432	0.000009	0.9995
06MY495H	24.00 W	0.002580	0.000004	0.9971	LIN # 3 6	0.000897	0.000006	0.9657	LIN #	0.002539	0.000010	0.9996
06MY495I	30.00 W	0.004614	0.000007	0.9974	LIN # 4 5	0.001292	0.000007	0.9812	LIN #	0.003612	0.000016	0.9997
06MY495J	35.00 W	0.003063	0.000010	0.9612	LIN #	0.001721	0.000006	0.9928	LIN #	0.003902	0.000016	0.9998
06MY495K	40.00 W	0.001886	0.000013	0.8972	LIN # 12	0.001126	0.000008	0.9750	LIN #	0.002156	0.000013	0.9995
06MY495L	50.00 W	0.001012	0.000009	0.8622	LIN #	0.001160	0.000008	0.9712	LIN #	0.003059	0.000010	0.9998
06MY495M	60.00 W	0.000342	0.000004	0.9519	LIN #	0.000480	0.000005	0.9152	LIN #	0.001337	0.000007	0.9996

Intercept Values (cont.)			^{39}Ar	1σ	r2		^{40}Ar	1σ	r2	
06MY495A	4.00 W	EXP #	0.020761	0.000038	0.9998	EXP #	7.217916	0.004680	0.9997	EXP # 1 8 9
06MY495B	8.00 W	EXP #	0.070234	0.000050	0.9993	EXP # 1 11 12	3.304948	0.001443	0.9999	EXP # 1 11 12
06MY495C	12.00 W	EXP #	0.195936	0.000240	0.9983	EXP # 4	7.997700	0.004668	0.9998	EXP # 1 6 12
06MY495D	16.00 W	EXP #	0.112242	0.000075	0.9996	EXP #	3.417831	0.000945	0.9999	EXP # 1
06MY495E	18.00 W	EXP #	0.061959	0.000051	0.9995	EXP # 1 2	2.059325	0.001441	0.9997	EXP # 1
06MY495F	20.00 W	EXP #	0.114601	0.000059	0.9998	EXP # 11	3.377501	0.002796	0.9996	EXP # 1 11
06MY495G	22.00 W	EXP #	0.071485	0.000050	0.9995	EXP # 12	2.192970	0.001030	0.9998	EXP # 1
06MY495H	24.00 W	EXP #	0.112016	0.000097	0.9993	EXP # 4	3.525960	0.002249	0.9997	EXP # 1
06MY495I	30.00 W	EXP #	0.172003	0.000119	0.9996	EXP # 1 10	5.473306	0.004509	0.9995	EXP # 1 11
06MY495J	35.00 W	EXP #	0.209511	0.000189	0.9992	EXP #	5.838661	0.005098	0.9995	EXP # 1
06MY495K	40.00 W	EXP #	0.112516	0.000119	0.9991	EXP # 1	3.133209	0.003477	0.9991	EXP # 1
06MY495L	50.00 W	EXP #	0.177621	0.000146	0.9995	EXP # 1	4.447468	0.003562	0.9995	EXP # 1
06MY495M	60.00 W	EXP #	0.079685	0.000088	0.9991	EXP # 1	1.927556	0.002843	0.9987	EXP # 1 2

TABLE III | **Data Tables and Figures of whole-rock groundmass $^{40}Ar/^{39}Ar$ dating from Cerro Prieto lamprophyre.**

Incremental Heating			$^{36}Ar(a)$	$^{37}Ar(ca)$	$^{38}Ar(cl)$	$^{39}Ar(k)$	$^{40}Ar(r)$	Age ± 2s (Ma)	$^{40}Ar(r)$ (%)	$^{39}Ar(k)$ (%)	K/Ca ± 2σ
06MY001A	47.50 W		0.00158	0.00452	0.00000	0.00925	0.14797	88.73 ± 145.98	24.01	0.00	0.881 ± 6.109
06MY001B	54.60 W		0.37733	4.41144	0.01848	2.25519	22.29561	55.38 ± 2.49	16.66	0.92	0.220 ± 0.015
06MY001D	66.50 W	4	0.69047	43.19189	0.00000	30.46993	813.33264	145.78 ± 0.57	79.94	12.45	0.303 ± 0.020
06MY001E	71.00 W	4	0.37354	46.30939	0.00000	51.19093	1314.72516	140.48 ± 1.22	92.25	20.91	0.475 ± 0.032
06MY001F	69.60 W	4	0.05656	7.49035	0.00000	10.67103	297.25972	151.88 ± 0.96	94.67	4.36	0.613 ± 0.041
06MY001G	70.60 W	4	0.04760	9.01638	0.00000	13.10824	358.14206	149.08 ± 0.78	96.22	5.35	0.625 ± 0.042
06MY001H	70.90 W	4	0.03441	6.59365	0.00000	10.01328	262.09254	143.06 ± 0.67	96.26	4.09	0.653 ± 0.044
06MY001I	71.20 W	4	0.03624	7.79773	0.00000	11.14448	300.75665	147.33 ± 0.67	96.56	4.55	0.615 ± 0.041
06MY001J	71.60 W	4	0.07916	18.24408	0.00000	23.68318	708.16364	162.54 ± 0.66	96.80	9.67	0.558 ± 0.037
06MY001K	71.70 W	4	0.02159	5.52183	0.00000	7.31343	194.30144	145.13 ± 0.59	96.82	2.99	0.570 ± 0.038
06MY001L	71.90 W	4	0.01851	4.71837	0.00000	6.33139	158.95930	137.44 ± 0.75	96.67	2.59	0.577 ± 0.039
06MY001M	72.00 W	4	0.01586	4.05283	0.00000	5.47598	133.62915	133.73 ± 0.43	96.61	2.24	0.581 ± 0.039
06MY001N	72.80 W	4	0.03218	9.47721	0.00000	11.30837	299.69249	144.78 ± 0.73	96.92	4.62	0.513 ± 0.035
06MY001O	73.00 W	4	0.01979	5.35309	0.00000	6.77520	162.70663	131.68 ± 0.62	96.53	2.77	0.544 ± 0.037
06MY001P	73.40 W	4	0.01332	3.54812	0.00000	4.36438	96.72072	121.85 ± 0.66	96.08	1.78	0.529 ± 0.036
06MY001Q	59.50 W	4	0.00122	0.21483	0.00017	0.31737	5.66945	98.86 ± 0.81	94.01	0.13	0.635 ± 0.047
06MY001R	60.50 W	4	0.00861	1.72661	0.00000	2.91285	69.36249	130.61 ± 0.53	96.46	1.19	0.725 ± 0.049
06MY001T	63.80 W	4	0.01986	5.82412	0.00000	5.90678	118.20828	110.39 ± 0.44	95.27	2.41	0.436 ± 0.030
06MY001U	67.30 W	4	0.09291	23.93424	0.00000	23.06322	400.20615	96.10 ± 0.30	93.58	9.42	0.414 ± 0.028
06MY001V	100.00 W		0.08000	18.20359	0.00099	18.48704	301.51325	90.47 ± 0.28	92.73	7.55	0.437 ± 0.030
		Σ	2.02076	225.63426	0.01963	244.80151	6017.88477				

Information on Analysis		Results	40(r)/39(k) ± 2σ		Age ± 2σ (Ma)		MSWD	39Ar(k) (%,n)	K/Ca ± 2σ
Sample	VU54-C15	**Error Plateau**	22.9773	± 1.9662	126.18	± 10.45	5588.45	91.52	0.501 ± 0.058
Material	lamprophyre			± 8.56%		± 8.28%		17	
Location	Betic Zone				External Error	± 10.75	2.12	Statistical T ratio	
Analyst	jc/jr				Analytical Error	± 10.43	74.7559	Error Magnification	
Project	VU54	**Total Fusion Age**	24.5827	± 0.0547	134.68	± 0.83		20	0.467 ± 0.011
Irradiation	VU54			± 0.22%		± 0.62%			
J-value	0.003153				External Error	± 2.82			
Standard	25.26				Analytical Error	± 0.29			